Physica A 392 (2013) 221–251

Contents lists available at SciVerse ScienceDirect

Physica A

journal homepage: www.elsevier.com/locate/physa

Traffic dynamics in empirical probe vehicle data studied with three-phase theory: Spatiotemporal reconstruction of traffic phases and generation of jam warning messages

Boris S. Kerner [a,*], Hubert Rehborn [a], Ralf-Peter Schäfer [b], Sergey L. Klenov [c], Jochen Palmer [a], Stefan Lorkowski [b], Nikolaus Witte [b]

[a] Daimler AG, RD/RTF, HPC: 050-G021, D-71059 Sindelfingen, Germany

[b] TomTom, TomTom Content Production Unit Berlin, An den Treptowers 1, D-12435 Berlin, Germany

[c] Moscow Institute of Physics and Technology, Department of Physics, 141700 Dolgoprudny, Moscow Region, Russia

ARTICLE INFO

Article history:
Received 9 May 2012
Received in revised form 22 June 2012
Available online 8 August 2012

Keywords:
Probe vehicle data
Traffic flow simulations
Three-phase traffic theory
Spatiotemporal traffic patterns
Phase transitions
Jam warning messages

ABSTRACT

Empirical and theoretical analyses of the spatiotemporal dynamics of traffic flow reconstructed from randomly distributed probe vehicle data are presented. For the empirical analysis, probe vehicle data generated by TomTom's navigation devices in the commercial TomTom's HD-traffic service as well as road detector data measured at the same road section are used. A stochastic microscopic (car-following) three-phase model is further developed for simulations of a real empirical complex spatiotemporal traffic dynamics measured over a three-lane long road stretch with several different bottlenecks. Physical features and limitations of simulations of real spatiotemporal traffic dynamics are revealed. Phase transition points between free flow (F), synchronized flow (S), and wide moving jam (J) are identified along trajectories of empirical and simulated probe vehicles randomly distributed in traffic flow. As predicted by three-phase theory, the empirical probe vehicle data shows that traffic breakdown is an F $\rightarrow$ S transition and wide moving jams emerge only in synchronized flow, i.e., due to S $\rightarrow$ J transitions. Through the use of the simulations, it has been found that already about 2% of probe vehicle data allows us to reconstruct traffic dynamics in space and time with an accuracy that is high enough for most applications like the generation of jam warning messages studied in the article.

© 2012 Elsevier B.V. All rights reserved.

1. Introduction

Empirical spatiotemporal characteristics of real vehicular traffic flow are of great importance for both the understanding of the physics of traffic and for the development of traffic flow theories and models. Up to now *spatiotemporal* characteristics of real traffic could be measured either through the use of road detectors or video cameras [1,2]. The advantage of measurements through the road detectors is that traffic can be measured over a long road stretch or even in the whole highway network (Fig. 1); the drawback of these measurements is that real spatiotemporal traffic dynamics between the detectors is not known. The advantage of video camera measurements is a fine microscopic reconstruction of individual vehicle trajectories in space and time; a problem of the measurements is that they are extremely expensive and, therefore,

* Corresponding author.
E-mail address: boris.kerner@daimler.com (B.S. Kerner).

0378-4371/$ – see front matter © 2012 Elsevier B.V. All rights reserved.
doi:10.1016/j.physa.2012.07.070

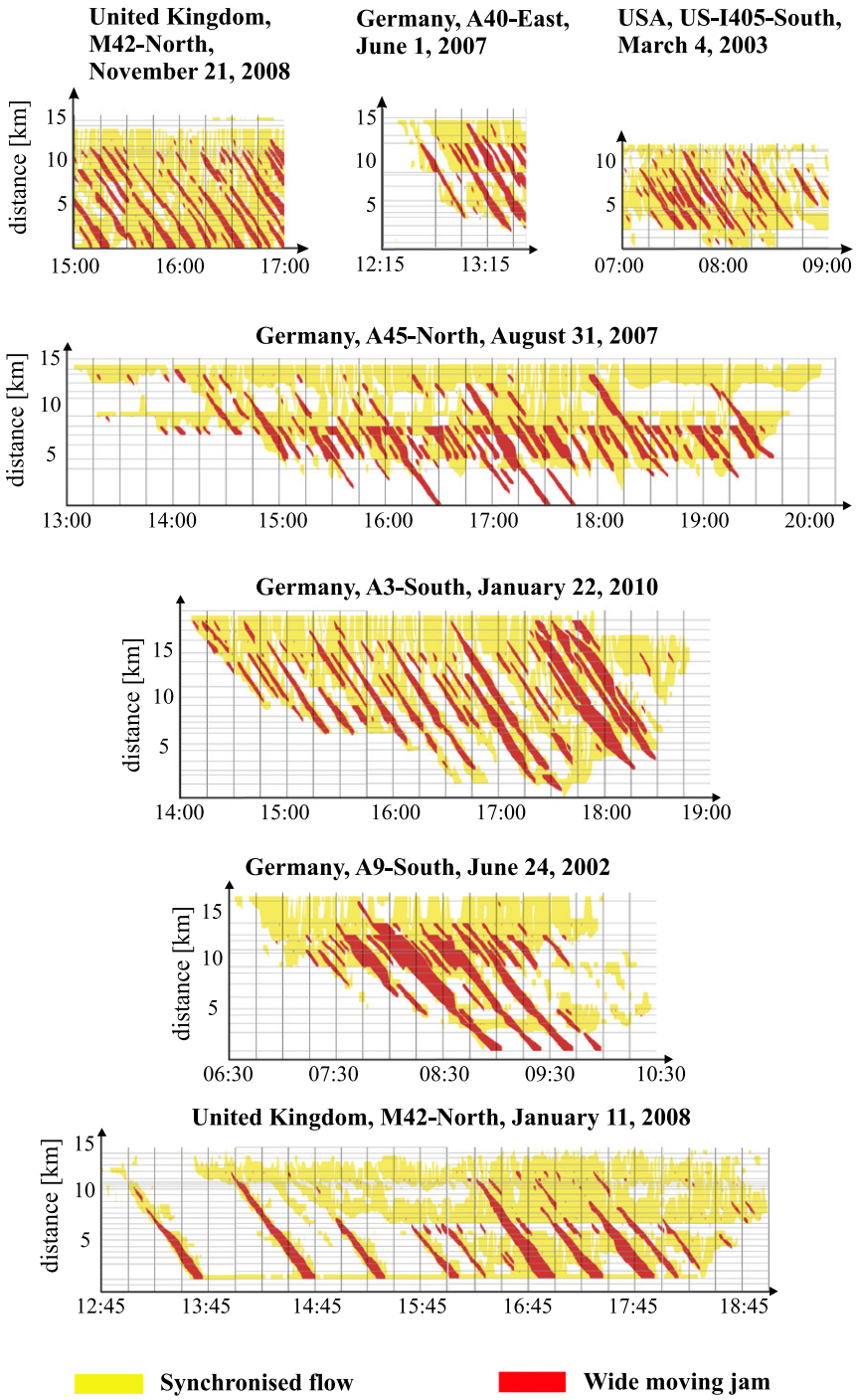

Fig. 1. Overviews of empirical examples of spatiotemporal congested patterns reconstructed and tracked by the ASDA and FOTO models using raw data measured by road detectors on different highways in the United Kingdom, Germany, and the USA. Explanations of the ASDA and FOTO models are given in Appendix C.1 of Appendix C.

they can be made for a very short road stretch (e.g., in the NGSIM-data [2], only 600–700 m long road sections of US roads) that does not usually permit us to understand the reason for traffic breakdown as well as does not allow us to reconstruct the whole spatiotemporal structure of a congested pattern. Although probe vehicle data (also called floating car data (FCD)) and data measured by mobile telephones could theoretically solve these problems, however, it was not possible (sending of the data to a control center is expensive) to collect enough probe vehicle data for reliable empirical measurements of the whole spatiotemporal traffic dynamics.

This situation has changed only recently through a breakthrough in the collection of mass real measured probe data from TomTom navigation devices used in vehicles and phone data from cellular networks (Vodafone data) available and stored at the TomTom's traffic center (www.tomtom.com). In this article, we study empirical vehicle probe data from TomTom navigation devices in the framework of three-phase theory introduced by Kerner [3,4]. We find that if the empirical probe vehicle data are analyzed with three-phase traffic theory [3–5], then a fine spatiotemporal structure of traffic flow patterns can be recognized in probe vehicle data.

The reason why we apply three-phase theory for this empirical data analysis is as follows. In empirical observations, spontaneous traffic breakdown at a highway bottleneck leading to congested traffic is a first-order local phase transition from free flow (F) to synchronized flow (S) (F $\rightarrow$ S transition) [4–6]. Rather than an F $\rightarrow$ S transition, in so-called *two-phase* traffic flow models explaining traffic breakdown through free flow instability [1,7] traffic breakdown is a local first-order phase transition from free flow to a wide moving jam (J) (F $\rightarrow$ J transition) (see Sec. 10.3 of the book [6]).

Because the two-phase models as well as other classical traffic flow theories and models cannot explain traffic breakdown as observed in real measured traffic data, Kerner introduced three-phase traffic theory [4,5] in which there are (i) the free flow, (ii) synchronized flow, and (iii) wide moving jam phases. The synchronized flow and wide moving jam phases associated with congested traffic are defined via the empirical definitions [S] and [J], respectively.

The definition [J] is as follows: A wide moving jam is a moving traffic jam, i.e., a localized structure of great vehicle density and low speed, spatially limited by two jam fronts, which exhibits the characteristic jam feature to propagate through bottlenecks while maintaining the mean velocity of the downstream jam front. This characteristic jam feature that follows from the definition [J] is called as the jam feature [J].

The definition [S] is as follows: Synchronized flow is congested traffic that does not exhibit the jam feature [J]; in particular, the downstream front of synchronized flow is often *fixed* at the bottleneck. Traffic data for the vehicle speeds measured with road detectors (1 min averaged data) illustrates the definitions [J] and [S] (Fig. 2(a)). There are two spatial–temporal patterns of congested traffic with low vehicle speeds in Fig. 2(a). One pattern of congested traffic propagates upstream with almost constant velocity of the downstream pattern front through the freeway bottleneck. According to the definition [J] this pattern of congested traffic belongs to the wide moving jam traffic phase. In contrast, the downstream front of the other pattern of the congested traffic is fixed at the bottleneck. According to the definition [S] this pattern of congested traffic belongs to the synchronized flow traffic phase (Fig. 2(a) and (b)). It should be mentioned that a congested pattern in which congested traffic consists of synchronized flow only is called a synchronized pattern (SP), whereas a congested pattern consisting of both phases of congested traffic, synchronized flow and wide moving jam, is called a general pattern (GP).

In Sect. 6.1 of [6] it has been shown that the definitions [S] and [J] are the origin of most hypotheses of three-phase theory and related three-phase microscopic models. First three-phase microscopic traffic flow models, which could show a first-order F $\rightarrow$ S transition and resulting congested patterns of three-phase theory, were introduced in Ref. [8,9]. Over time a number of three-phase traffic models have been developed (e.g., Ref. [10–46]).

It must be noted that the definitions [J] and [S] are non-local macroscopic ones and they are applicable only after macroscopic data has been measured in space and time, i.e., in an "off-line" study. This is because for the definitive distinction of the phases J and S through the definitions [J] and [S] a study of the propagation of traffic congestion through a bottleneck is necessary. This is often considered as a drawback of the traffic phase definitions. However, there are local microscopic criteria for the distinction between the phases J and S without a study of the propagation of congested traffic through a bottleneck. The microscopic criteria are as follows [47]: If in single-vehicle data related to congested traffic the "flow-interruption interval", i.e., a time headway between two vehicles following each other is observed, which is much longer than the mean time delay in vehicle acceleration from a wide moving jam (the latter is about 1.3–2.1 s), then the related flow-interruption interval corresponds to the wide moving jam phase. After all wide moving jams have been found through this criterion in congested traffic, all remaining congested states are related to the synchronized flow phase. In particular, results of the application of the microscopic criterion for the traffic phases allows us to show a qualitative difference between two different localized moving structures of three-phase theory, moving SPs (MSP) and wide moving jams, while the patterns propagate on a homogeneous road without bottlenecks (see Sec. IV.C of [42]).

The article is organized as follows: In Section 2, we describe empirical data as well as present the methodology of the data analysis. Simulations of single vehicle data based on real measured road inflow and outflow rates is performed in Section 3 based on the Kerner–Klenov stochastic microscopic three-phase traffic flow model. To perform these simulations as close as possible to real traffic and to understand the fundamental physical limitations of simulations of particular characteristics of empirical spatiotemporal features of traffic dynamics, in Appendix A we have also made a further development of the Kerner–Klenov model for a three-lane road with several on- and off-ramp bottlenecks in accordance with characteristics of a road section on which empirical probe vehicle data and road detector data have been measured. Recognition of fronts between different traffic phases through probe vehicles both in empirical and simulated probe vehicle data have been made in Section 4. This traffic phase recognition along vehicle trajectories has been used in Section 5 to generate jam danger warning messages in empirical and simulated probe vehicle data. Finally, we have reconstructed spatiotemporal regions of synchronized flow and wide moving jams from both empirical and simulated probe vehicle data in Section 6. To reach this goal, FOTO and ASDA models for pattern reconstruction from probe vehicle data have been further developed (Appendix B), which incorporate ideas of the FOTO and ASDA models for spatiotemporal traffic pattern reconstruction from road detector data (Appendix C).

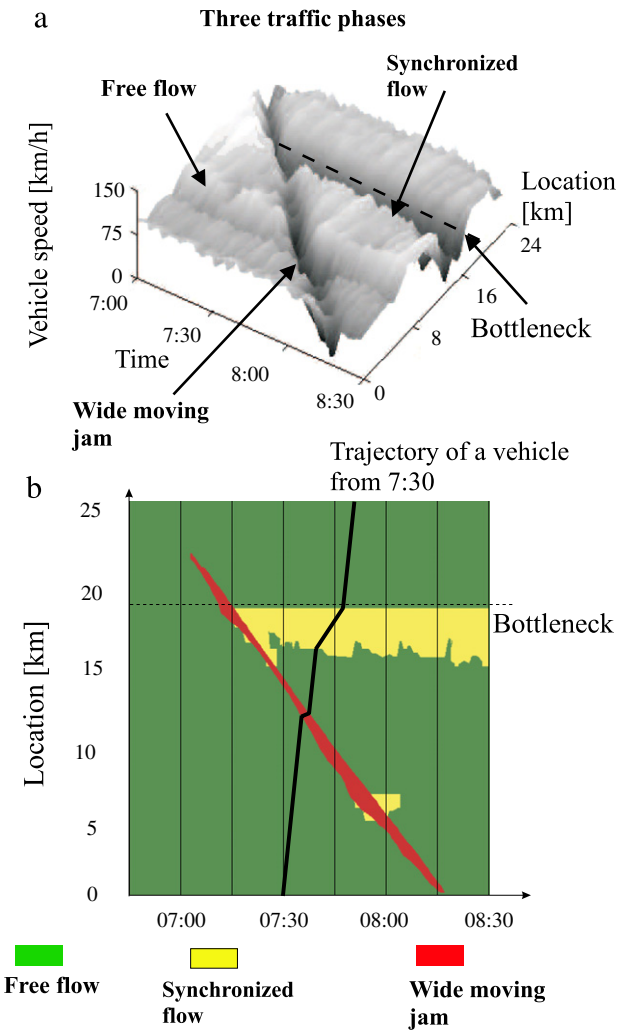

Fig. 2. Explanation of the traffic phase definitions in three-phase theory based on measured data of speed in time and space (a). (b) Representation of speed data in (a) on the time–space plane. Explanations of the approximate reconstruction of spatiotemporal traffic dynamics based on road detector measurements shown in this figure are given in Appendix C.2 of Appendix C.

2. Empirical data and methodology of data study

2.1. Empirical traffic data measured by road detectors and probe vehicles moving in traffic flow

There are two sources of real empirical data, which have been measured on the same days and road sections and that have been available for the study:

(i) TomTom GPS probe vehicle data (referred to as GPS-probe vehicle data) (Figs. 3(a), 4(a) and 5(a)). GPS-probe vehicle data has been obtained through TomTom's navigation devices: Each of the devices measures the vehicle co-ordinates and speed at the beginning of each time step Δt (at time $\Delta t = 10$ s), stores the result and sends a packet of 12 such measurements to the TomTom traffic server. Note that the choice of a relatively long time step Δt is associated with expensive communication charges for much shorter time steps (the latter could be possible up to time step 0.1 s).

(ii) Macroscopic (1-min averaged) data measured by road detectors (referred to as detector data) located at about 1 km distance from each other. The three-lane road section on which detector data is measured is about 30 km long; there are 31 sets of detectors in each lane of the main road and detectors in each of the off- and on-ramp lanes within intersections I1, I2, and I3 with other highways (Fig. 6(a)). To show overviews of the traffic dynamics in space and time, in Figs. 3(c), 4(b) and 5(b) the data has been processed through the FOTO and ASDA models (see Appendix C.1 of Appendix C), which make firstly the distinguishing of the three traffic phases at detector locations and secondly the reconstruction of the traffic phases between detector locations.

In addition, in Fig. 3(b) we present GSM (Vodafone) data of mobile telephones. It must be mentioned that GSM-probe vehicle data has *not* been available as raw data but in the form of figures only, therefore, the data could not be used in

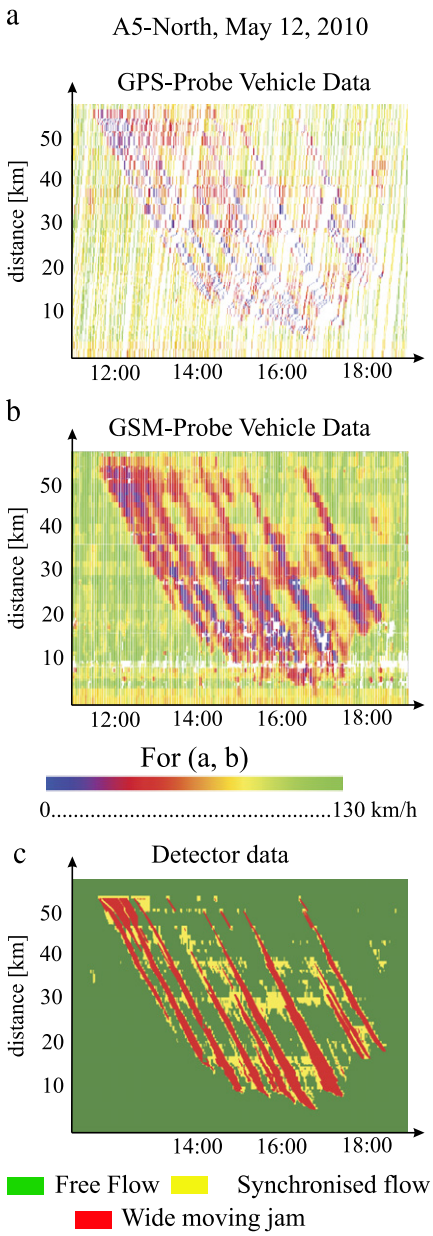

Fig. 3. Overviews of TomTom GPS-probe vehicle data (a), TomTom GSM-probe vehicle data (b), and road detector data (c) measured on 12th May, 2010 on A5-North on A5 highway in Germany within a congested pattern: (a, b) Vehicle trajectories in space and time; different colors (in on-line article version) along trajectories are related to different speeds. (c) The three traffic phases reconstructed with FOTO and ASDA models from raw road detector data.

this study; this data is shown for a visual comparison with probe vehicle and road detector data (Figs. 3(a), (c)). From this comparison, we can conclude that spatiotemporal structures of traffic patterns measured through three different data sources are qualitatively very similar.

2.2. Empirical data and methodology of data study

For a correct evaluation of any method for traffic phase reconstruction one needs single-vehicle data with the vehicle speed and location as time-functions measured along a vehicle trajectory while the vehicle moves though all traffic phases F, S, and J. However, currently such precise single-vehicle data measured in real traffic are not available. For this reason, in this article we will use the following methodology:

1. There is a database of the data measured during 1996–2010 by road detectors on a highway section shown in Fig. 6(a). We choose a representative data set from this empirical database (Fig. 5(b)). The data set exhibits spatiotemporal structures

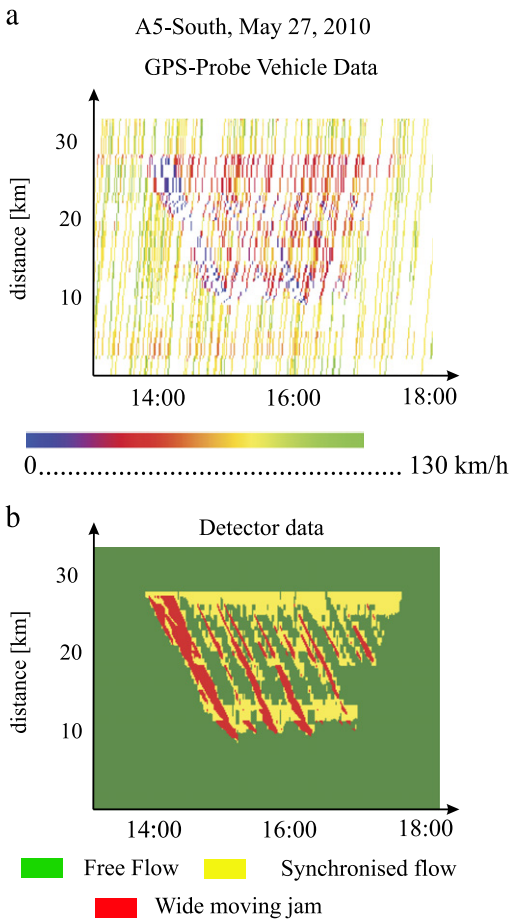

Fig. 4. Overviews of TomTom GPS-probe vehicle data (a) and road detector data (b) measured on 27th May, 2010 on A5-South highway in Germany within a congested pattern: (a) Vehicle trajectories in space and time. (b) The three traffic phases reconstructed with FOTO and ASDA models from raw road detector data.

of congested traffic that are common for all data measured on different highways in various countries (Fig. 1): Congested traffic consists of synchronized flow and wide moving jams that satisfy the phase definitions [S] and [J], respectively.

2. We simulate the empirical spatiotemporal traffic dynamics of the representative pattern (Figs. 3(c), 4(b) and 5(b)).
3. For an adequate comparison of the simulations and empirical data, in the simulated pattern shown in Fig. 7(a) a small percentage of the vehicles, which are randomly distributed within traffic flow, are considered probe vehicles (simulated floating car data). Such a choice of simulated vehicle trajectories of the probe vehicles is associated with empirical TomTom data that have also been measured by a small percentage of randomly distributed vehicles moving through real traffic pattern.
4. Phase transition points between free flow (F), synchronized flow (S), and wide moving jam (J) are identified along trajectories of probe vehicles. This procedure is made both for different percentages of simulated vehicle trajectories and for empirical TomTom probe vehicle data related to the same day (Fig. 5(a)).
5. Jam warning messages through the use of traffic phase identification along vehicle trajectories are generated both for empirical and simulated probe vehicle data.
6. The reconstruction of the spatiotemporal regions of the phases S and J from probe vehicle data is made for both empirical and simulated probe vehicle data.

3. Results of simulations of empirical spatiotemporal traffic dynamics measured on multi-lane highways

Many real highways in industrial countries have more than two lanes in one road direction. Due to a complex lane changing on such multi-lane highways and many on- and off-ramp bottlenecks as well as very different driver and vehicle characteristics in real traffic the following question arises:

- What can be the fundamental physical limitations in simulations of particular characteristics of empirical spatiotemporal features of traffic dynamics measured on a particular day on a multi-lane highway?

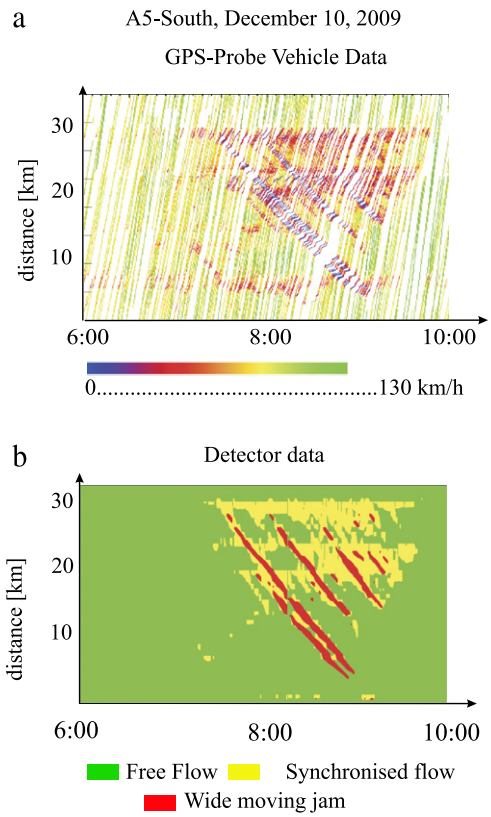

Fig. 5. Overviews of TomTom GPS-probe vehicle data (a) and road detector data (b) measured on 10th December, 2009 on A5-South highway in Germany within a congested pattern: (a) Vehicle trajectories in space and time. (b) The three traffic phases reconstructed with FOTO and ASDA models from raw road detector data.

We will try to answer this complex question through simulations of the representative empirical pattern (Fig. 5(b)) measured on three-lane road with on- and off-ramp bottlenecks. To make simulations as close to reality as possible we perform a further development of the Kerner–Klenov stochastic microscopic three-phase traffic flow model, which has initially been formulated and used for traffic simulations on single-lane and two-lane roads [14,48,49,51]. In these simulations, we apply a model of the three-lane road section of the A5 freeway in Germany on which the representative pattern has been measured; in addition, we use in these simulations empirical inflow and outflow rates taking into account percentages of long vehicles in these in- and outflows measured by road detectors (Fig. 6(b)).

For a more easy paper understanding, we will present and discuss the three-lane stochastic Kerner–Klenov three-phase microscopic model in Appendix A.

Simulations with this model show the following results:

1. As in the real data used, in all simulations traffic breakdown at a bottleneck is always an F $\rightarrow$ S transition, whereas wide moving jams emerge spontaneously in synchronized flow only (S $\rightarrow$ J transitions).
2. To simulate traffic breakdown in a heterogeneous flow at a bottleneck on a multi-lane road as close as possible both qualitatively and quantitatively to measured data, specific parameters of the bottlenecks should be chosen. In particular, as explained in Appendix A, the road lengths L_d upstream of an on-ramp and L_m within the on-ramp merging region (Fig. A.2(a)) exhibit the great effect on traffic breakdown and resulting synchronized flow at on-ramp bottlenecks. The physics of this result is as follows: Within these road sections, the personal vehicles moving in the right lane on the main road try to change to middle the lane, and the vehicles moving in the middle lane try to change to left the lane. The shorter these road sections, the greater speed fluctuations due to lane changing at the same flow rate and, therefore, traffic breakdown occurs on average at the smaller flow rates. Similarly, for off-ramp bottlenecks the road lengths L_d upstream of an off-ramp and within the off-ramp merging region $L_c + L_m$ (Fig. A.2(b)) exhibit the great influence on traffic breakdown and resulting synchronized flow at off-ramp bottlenecks. This is because within these road regions the vehicles that are not going to the off-ramp change from the right to the middle lane and from the middle to the left lane. Thus the shorter these road lengths, the greater on average the speed fluctuations that lead easier to traffic breakdown.
3. Through an appropriated choice of these bottleneck parameters we have been able to simulate a spatiotemporal congested pattern (Fig. 7(a)) that is very close both in time and space to the empirical pattern reconstructed from detector

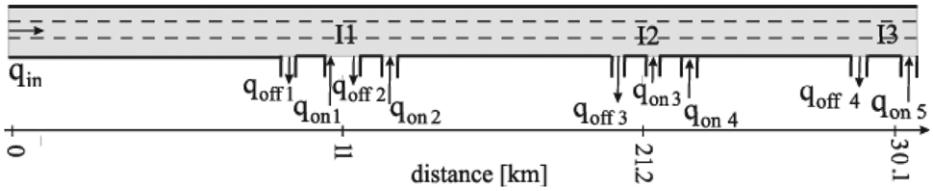

(a) I1: Friedberg, I2: Bad Homburger Kruez, I3: Nordwestkreuz.

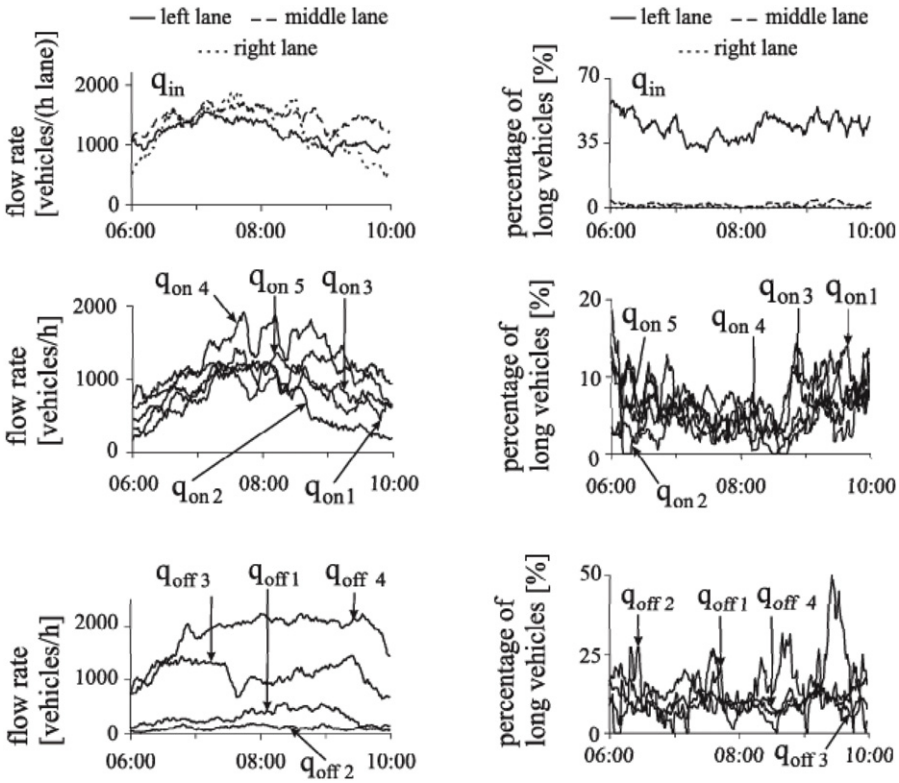

(b) Measured inflows and outflows used in simulations.

Fig. 6. Empirical inflows and outflows used in simulations: (a) Simplified schema of three-lane road section of A5-South highway in Germany on which both probe vehicle data and detector data presented in Fig. 5 were measured on 10th December, 2009 (a). (b) Measured time-functions of inflows and outflows (left) with percentages of long vehicles (right) used in simulations. In (a), locations of on-ramps $x_{\mathrm{on}\,i}$, $i = 1, 2, \ldots, 5$ are 11.085, 11.789, 21.522, 21.86, 30.19 km, respectively; locations of off-ramps $x_{\mathrm{off}\,j}$, $j = 1, 2, 3, 4$ are 10.674, 11.366, 18.612, 27.768 km, respectively.

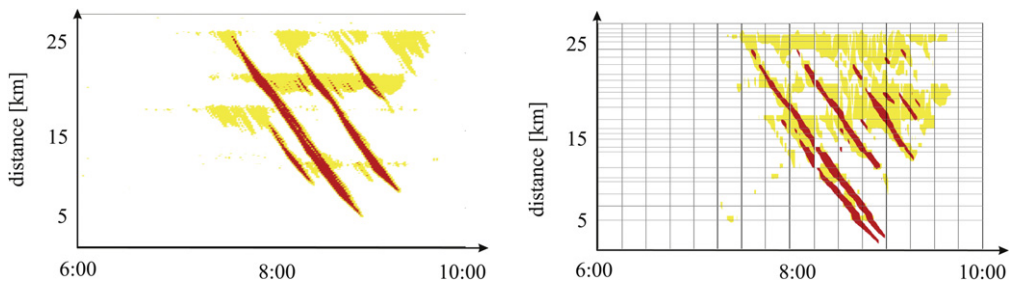

(a) Realization 1. (b) Measured data processed via ASDA/FOTO.

Fig. 7. Comparison of realization 1 of microscopic simulations (a) with real measured data processed via the ASDA and FOTO methods (b). Figure (b) is taken from Fig. 5(b).

data through the use of the ASDA and FOTO models (Fig. 7(b)). In accordance with three-phase theory [6], this pattern is an example of an expanded GP (EGP).

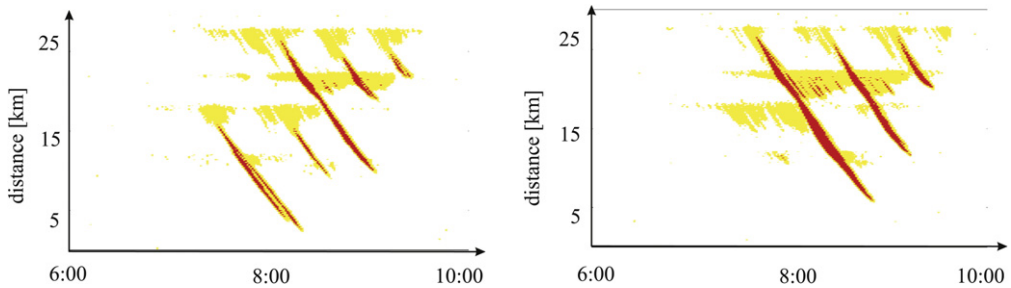

(a) Realization 2. (b) Realization 3.

Fig. 8. Two different realizations 2 and 3 of microscopic simulations.

4. However, we should mention that the time instant of traffic breakdown at a bottleneck (F $\rightarrow$ S transition) and the spatiotemporal distribution of traffic variables within the emergent synchronized flow are random characteristics, which can be different in different simulation realizations (runs). These different realizations have been made at the same inflow and outflow rates and other boundary conditions, however, at different initial values of model fluctuations, i.e., different initial values rand() in the model (see model functions in Appendix A). In two realizations 2 and 3 shown in Fig. 8(a) and (b), the maximum deviation of time instances of traffic breakdown at the bottlenecks from the associated values found in realization 1 (Fig. 7(a)) is about 10 min.
5. The time instant of the emergence of a wide moving jam in synchronized flow is also a random value, which can be different in different simulation realizations (runs). Moreover, in contrast with traffic breakdown that occurs in different simulation realizations at almost the same location in a neighborhood of a bottleneck, locations of the emergence and dissolution of wide moving jams are random values. The differences in time instants and locations of S $\rightarrow$ J transitions can be very significant in simulation realizations. In particular, some of the wide moving jams that appear in some of the realizations do not occur in other ones (compare realization 1 (Fig. 7(a)) with realizations 2 and 3 (Fig. 8)). In addition, we should mention that the jam dissolution is also a random pattern characteristic that is different in different simulation realizations.

These theoretical features of phase transitions found in different simulation realizations are qualitatively the same as those in the empirical database measured on the highway section under consideration over many years. It has been found that very different sequences of wide moving jams within GPs are observed on different days under very similar boundary conditions, i.e., when time-dependences of the inflow rate to the section, the flow rates to on-ramps, and the flow rates to off-ramps on the section are close to each other [5].

The emergence of wide moving jams at random time instants in synchronized flow and therefore at different road locations within the synchronized flow is explained in three-phase theory by the random occurrence of nuclei (critical speed disturbances) for wide moving jam emergence in synchronized flow (see Sec. 5.2 of [6]). As mentioned above, in different simulation realizations initial distributions of space gaps between vehicles on the road section at the beginning of simulations (i.e., at $t = 0$) causes a considerable change in the microscopic vehicle dynamics. This changes the nucleation dynamics of wide moving jams in synchronized flow. From a comparison of different realizations simulated with the model, we can conclude that simulation realization 1 (Fig. 7(a)) is one of the most closest to the empirical pattern (Fig. 7(b)) measured through the use of road detectors. Therefore, we use realization 1 (Fig. 7(a)) for further theoretical analysis of simulated microscopic data.

4. Recognition of fronts between different traffic phases through probe vehicles

4.1. Transition points between three traffic phases

For further analysis we firstly introduce the term *transition point* (point for short) for a phase transition between two different traffic phases along a trajectory of a probe vehicle and explain a qualitative difference between this transition point along a vehicle trajectory and phase transition in traffic. A point for a phase transition between two different traffic phases along a trajectory of a probe vehicle gives a road location and a time instant at which the phase transition is just observed by a driver of the associated probe vehicle. This point is related to a front that separates these two traffic phases. In particular, it is possible to distinguish the following points for transitions between different traffic phases along a vehicle trajectory (Fig. 9):

(a) Transition point from free flow to synchronized flow (denoted by F_S transition),
(b) transition point from synchronized flow to free flow (S_F transition),
(c) transition point from free flow to a wide moving jam (F_J transition),
(d) transition point from synchronized flow to a wide moving jam (S_J transition),

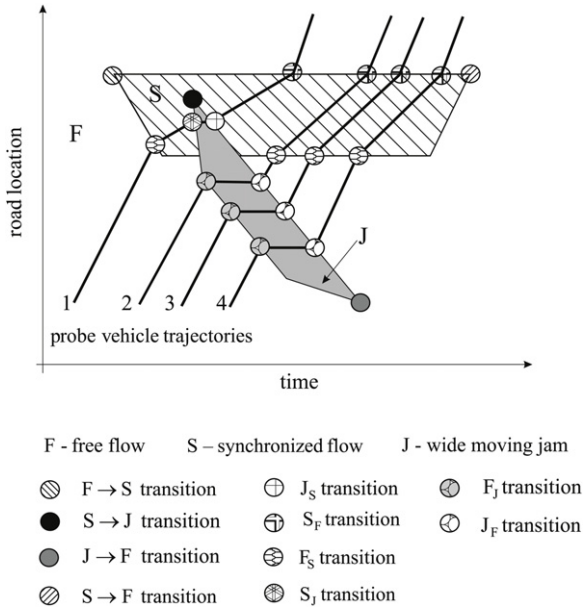

Fig. 9. Qualitative explanation of the difference between transition points for phase transitions along trajectories of four probe vehicles and phase transitions in traffic. White regions—free flow (F), a dashed region—synchronized flow (S), gray region—wide moving jam (J).

Table 1
Model for an approximate detection of phase transition points along a vehicle trajectory.

Phase transition points	Conditions for speed	Conditions for time interval
F_S	$v < v_{FS}$	$T > T_{FS}$
F_J	$v < v_{FJ}$	$T > T_{FJ}$
S_F	$v > v_{SF}$	$T > T_{SF}$
S_J	$v < v_{SJ}$	$T > T_{SJ}$
J_F	$v > v_{JF}$	$T > T_{JF}$
J_S	$v > v_{JS}$	$T > T_{JS}$

(e) transition point from a wide moving jam to free flow (J_F transition),
(f) transition point from a wide moving jam to synchronized flow (J_S transition).

It must be stressed that there is a qualitative difference between phase transitions in traffic and points for phase transitions along vehicle trajectories at which drivers observe phase transitions while moving through a congested pattern. Moving through a congested pattern, rather than an initial phase transition, a driver usually observes a transition between different traffic phases upstream and downstream of the front separating these traffic phases. This is qualitatively explained and shown in Fig. 9: An F → S transition, which leads to the emergence of synchronized flow and subsequent propagation of the front between two traffic phases F and S, has occurred earlier and at another road location than a location at which a driver of the probe vehicle 1 encounters the front between the phases F and S (transition point for F_S transition along the trajectory 1 in Fig. 9). An S → J transition, which leads to the emergence of a wide moving jam within synchronized flow and subsequent propagation of the upstream front of a wide moving jam, i.e., the front between two traffic phases S and J, has also occurred earlier and at another road location than a location at which the driver encounters the jam (see for example, point for S_J transition on the trajectory 1 in Fig. 9).

Thus, transition points on a vehicle trajectory at which the above-mentioned phase transitions (a)–(f) can be identified are usually not associated with the location and time instant at which phase transitions have initially occurred in traffic flow. For this reason, phase transitions are denoted by F → S transition, S → F transition, etc. In contrast, transition points for phase transitions along vehicle trajectories of probe vehicles are denoted by F_S transition, S_F transition, etc. (see items (a)–(f) above) (Fig. 9).

4.2. Recognition of transitions points along vehicle trajectories

A model for an approximate identification of a phase transition point from an initial traffic phase to another one along the trajectory of a probe vehicle moving in traffic flow is based on the condition that during a time interval T that is longer than a given threshold time interval the vehicle speed v along a trajectory becomes lower or higher than a given threshold speed for this phase transition point. The complete model is presented in Table 1, whereas model parameters that have been used for simulations are given in Table 2, respectively.

Table 2
Parameters of the model for an approximate detection of phase transition points along a vehicle trajectory used in this article.

Threshold speeds	Values (km/h)	Threshold time intervals	Values (s)
v_{FS}	60	T_{FS}	15
v_{FJ}	15	T_{FJ}	25
v_{SF}	65	T_{SF}	10
v_{SJ}	10	T_{SJ}	25
v_{JF}	60	T_{JF}	10
v_{JS}	20	T_{JS}	20

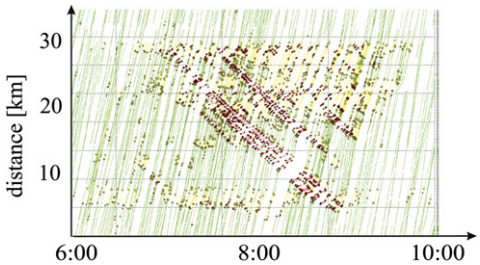

Fig. 10. Application of model (Tables 1 and 2) for the identification of transition points between different phases along empirical probe vehicle trajectories shown in Fig. 5 (a).

It should be noted that this model determines a phase transition point *only*; in other words, in the model it is assumed that an initial traffic phase in which a vehicle moves is known (as a rule, before a vehicle approaches a congested pattern it moves in free flow, i.e., usually the initial traffic phase on the vehicle trajectory studied with the model is free flow). To illustrate this, we consider an example of a vehicle moving with the speed 62 km/h during 60 s; this speed is between threshold points for phase transition points and, therefore, could be related to a free phase (if the vehicle has formerly moved in a free flow) or synchronized flow (if the vehicle has formerly moved in a synchronized flow).

Unrealistic frequent changes in traffic phases along a vehicle trajectory that could be caused by oscillations of the vehicle speed crossing over two or more threshold speeds are avoided in the model through the use of chosen threshold time intervals (Tables 1 and 2). These threshold time intervals have been found from the model validation, which has been made from a comparison of phase transition points found with the model and with the use of macroscopic and microscopic traffic phase definitions made in three-phase theory [6].

4.3. Transition points between different traffic phases in empirical data

To use the above model for the recognition of the transition points in empirical probe vehicles data measured by TomTom devices (Fig. 5(a)), firstly the microscopic speed along vehicle trajectories is approximately found through the linear approximation between measurements of the single vehicle speed and coordinates made with time steps $\Delta t = 10$ s (see Section 2.1). Then the model presented in Tables 1 and 2 is applied for each vehicle trajectory to find the transition points between different traffic phases along each of the vehicle trajectories. The result is shown in Fig. 10 in which each point is related to a road location at which a vehicle passes a phase front that separates two different traffic phases. Therefore, points associated with a traffic phase determine spatiotemporal boundaries between which the phase exists in space and time as shown in Fig. 10: the phase F—white regions, S—yellow, J—red (colors are related to the on-line paper version).

4.4. Simulations of spatiotemporal traffic dynamics for different penetration rate of probe vehicle data

Simulations allow us to find the dependence of the recognition of transition points between different traffic phases on the penetration rate of probe vehicle data randomly distributed in traffic flow. Indeed, after the congested pattern has been found in the microscopic simulations (Fig. 7(a)), we have information about vehicle trajectories of all vehicles moving through the pattern. We can assume that some of these vehicles are probe vehicles whose trajectories are available through V2X-communication (vehicle-to-vehicle and/or vehicle-to-infrastructure communication). We designate the percentage of these probe vehicles by η and assume that the probe vehicles are randomly distributed between all other vehicles. Vehicle trajectories of such probe vehicles at $\eta = 2\%$, $\eta = 0.5\%$, and $\eta = 0.25\%$ are presented in Fig. 11 (left).

Results of the application of the model presented in Table 1 to trajectories of probe vehicles shown in Fig. 11 (left) at different percentages of probe vehicles $\eta = 2\%$, $\eta = 0.5\%$, and $\eta = 0.25\%$ are presented in Fig. 11 (right), respectively. We can see that probe vehicles reconstruct many important features of spatiotemporal congested patterns already at the penetration rate of the vehicles of about $\eta = 0.5\%$.

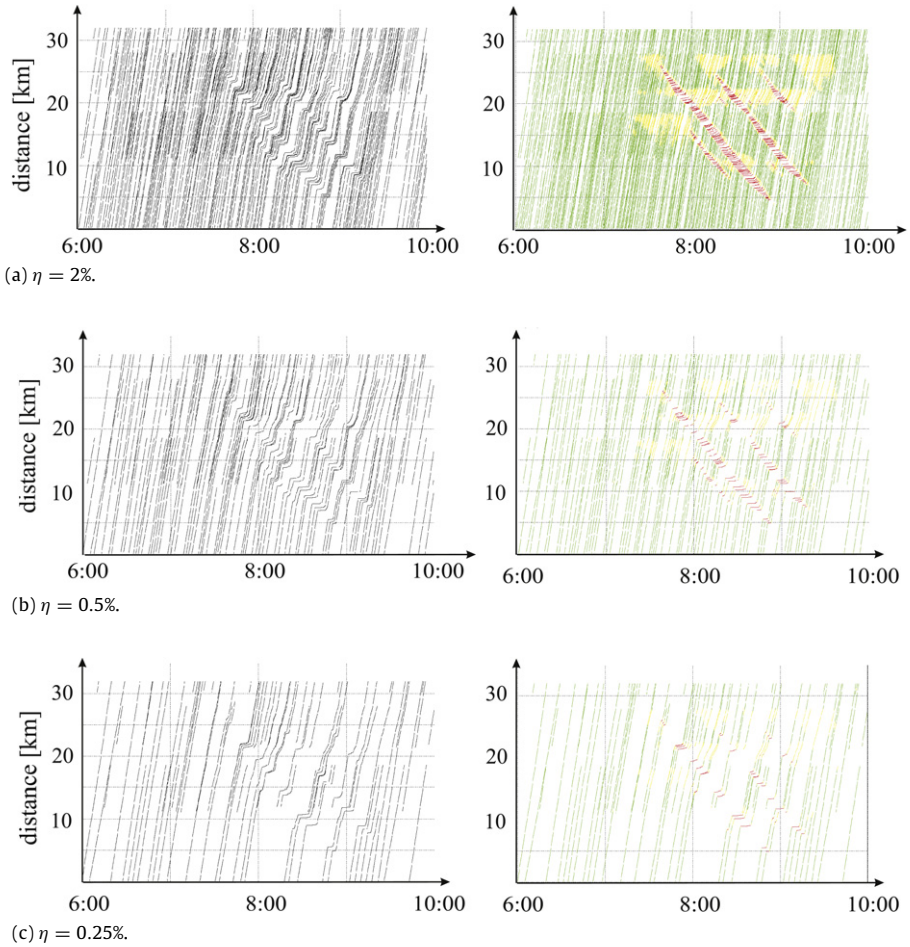

(a) $\eta = 2\%$.

(b) $\eta = 0.5\%$.

(c) $\eta = 0.25\%$.

Fig. 11. Trajectories of probe vehicles within the pattern shown in Fig. 7(a) (figures left) and results of the identification of transition points between different phases (figures right): (a)–(c) Percentage of probe vehicles $\eta = 2\%$ (a), $\eta = 0.5\%$ (b), and $\eta = 0.25\%$ (c).

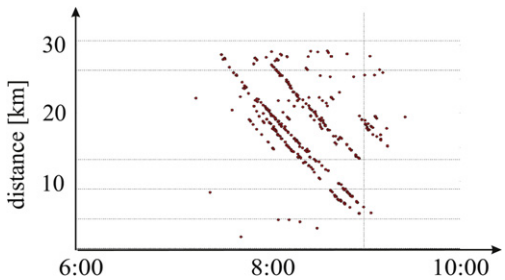

Fig. 12. Reconstruction of upstream fronts of wide moving jams based on traffic phase identification along empirical probe vehicle data shown in Fig. 10.

5. Generation of jam warning messages

5.1. Jam warning generation based on empirical probe vehicle data

Traffic phase identification along a probe vehicle trajectory explained above allows us to generate jam warning messages as follows: (i) A jam warning message is generated by a probe vehicle when either a F_J transition (transition from free flow to wide moving jam) or an S_J transition (transition from synchronized flow to wide moving jam) is identified along the vehicle trajectory. Then a sequence of these jam warning messages generated by all probe vehicles (Fig. 12) allows us to distinguish a spatiotemporal behavior of the propagation of the jam upstream front on the road. The upstream jam front propagation can be used for the warning of all other vehicles moving upstream of the jam front.

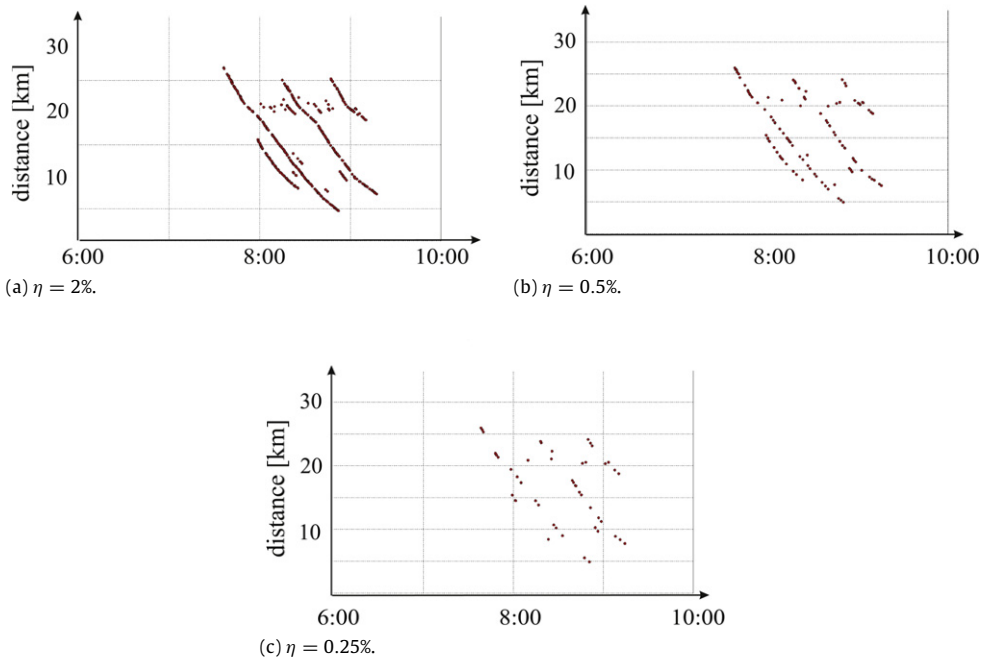

Fig. 13. Detection of upstream jam fronts ("jam warning messages") with different percentage of simulated probe vehicles: (a–c) Percentage of probe vehicles $\eta = 2\%$ (a), $\eta = 0.5\%$ (b), and $\eta = 0.25\%$ (c).

Because we have both TomTom GPS probe vehicle data (Fig. 5(a)) and empirical data measured by road detectors, we can calculate the penetration rate of the probe vehicle data in traffic flow measured on 10th December, 2009 on the section of A5 highway under consideration (Fig. 6(a)). We find that at location $x = 0$ km in Fig. 6(a) the total flow rate averaged across the highway and during the time interval from 7:00 to 10:00 is about 4000 vehicles/h. The average number of TomTom GPS probe vehicle data during the same time interval at this location is 41 probe vehicle data. Thus the average penetration rate of TomTom GPS probe vehicle data (Fig. 5(a)) in traffic flow data is about 1%.

5.2. Dependence of jam warning messages on penetration rate of probe vehicle data

As mentioned above the empirical probe vehicle data that are available in this study are related to the average penetration rate 1%. Through the use of simulated trajectories of probe vehicles randomly distributed in traffic flow (Fig. 11), we can find the dependence of jam warning messages on penetration rate of probe vehicle data (Fig. 13).

When a synchronized flow speed is low enough (a threshold synchronized flow speed can be a parameter stored in probe vehicles), then a warning message like "low speed traffic ahead" can be generated by probe vehicles if the vehicles identify a F_S transition (transition from free flow to synchronized flow) (Fig. 14). The propagation of the front of the transition recognized by the probe vehicles can also be used for the warning of all other vehicles moving upstream of the synchronized flow front.

The model of traffic phase identification allows us also to generate messages indicating the possibility of vehicle acceleration from a wide moving jam to either synchronized flow (J_S transition) or to free flow (J_F transition) (Fig. 15). The propagation of the associated front of vehicle escaping from the jam found though the probe vehicles can help other vehicles estimate the time-to-acceleration from the jam. This can be important for different ITS applications, for example, hybrid vehicle control.

5.3. Traffic phases in different road lanes identified through simulated probe vehicle data

In accordance with empirical data and microscopic theory of multi-lane traffic [50], in simulations applying the identification of traffic phases along probe vehicle trajectories separately for each of the road lanes we find that locations for phase transitions in different lanes can be very different and, therefore, at the same road location in different road lanes different traffic phases can occur (Fig. 16).

Thus, when a greater penetration rate of probe vehicles will be available and a lane precise technology for warning messages will be used, the model of the identification of traffic phases along vehicle trajectories can be used for such a lane-precise generation of warning messages either of F_J (Fig. 17) and S_J transitions or F_S and S_F transitions (Fig. 18) or else J_S and J_F transitions discussed above.

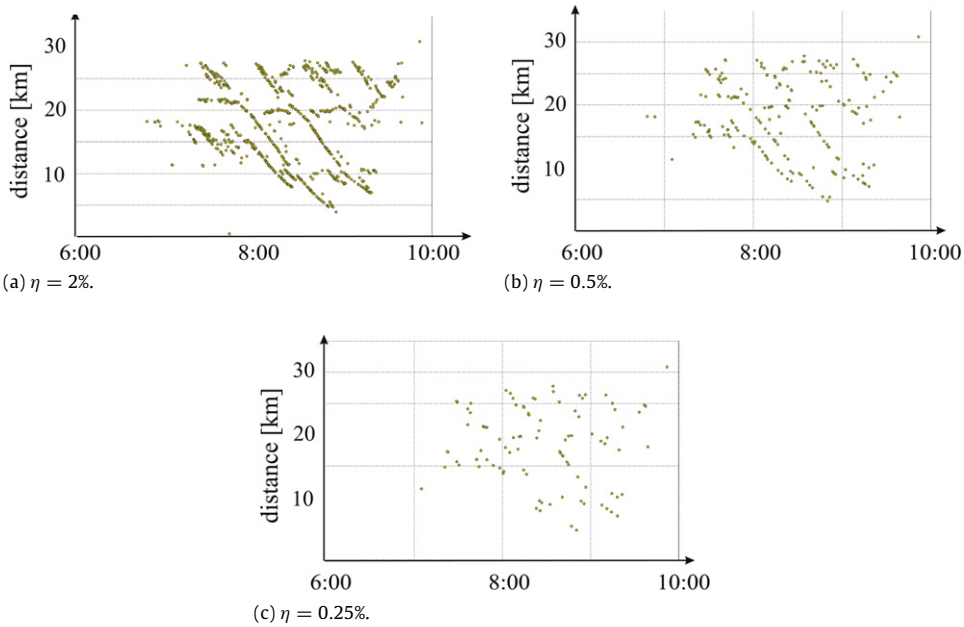

(a) $\eta = 2\%$. (b) $\eta = 0.5\%$.

(c) $\eta = 0.25\%$.

Fig. 14. Detection of transition ("synchronized flow front warning messages") with different percentage of probe vehicles: (a–c) Percentage of probe vehicles $\eta = 2\%$ (a), $\eta = 0.5\%$ (b), and $\eta = 0.25\%$ (c).

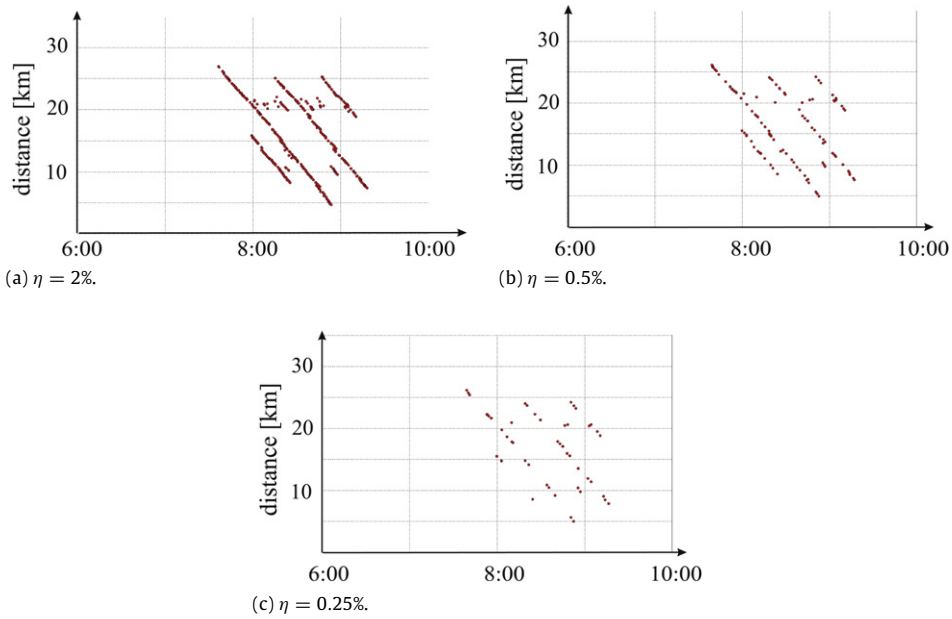

(a) $\eta = 2\%$. (b) $\eta = 0.5\%$.

(c) $\eta = 0.25\%$.

Fig. 15. Detection of downstream jam fronts ("jam end messages") with different percentage of probe vehicles: (a–c) Percentage of probe vehicles $\eta = 2\%$ (a), $\eta = 0.5\%$ (b), and $\eta = 0.25\%$ (c).

6. Traffic phases in space and time reconstructed from probe vehicle data

After the transition points for phase transitions have been identified, spatiotemporal regions of synchronized flow and wide moving jams can be reconstructed. One might have the impression that if there is a high enough penetration rate of probe vehicles, a simple connection of the associated transition points on each of the vehicle trajectories would reconstruct these regions of synchronized flow and wide moving jams with a good enough accuracy. At some very high penetration rate η this might be indeed possible as this has been seen in Fig. 7(a) and 8 for $\eta = 100\%$. In general, however, there can be several regions of synchronized flow and wide moving jams that are separated from each other.

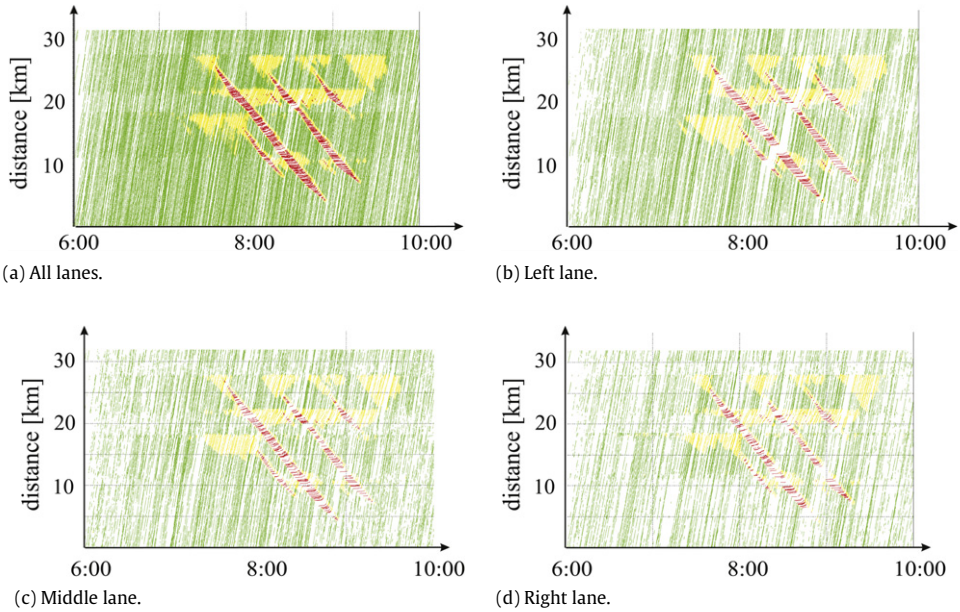

Fig. 16. Results of the identification of transition points between different phases in different road lanes with $\eta = 5\%$ of probe vehicles: (a) All lanes. (b) Left lane. (c) Middle lane. (d) Right lane.

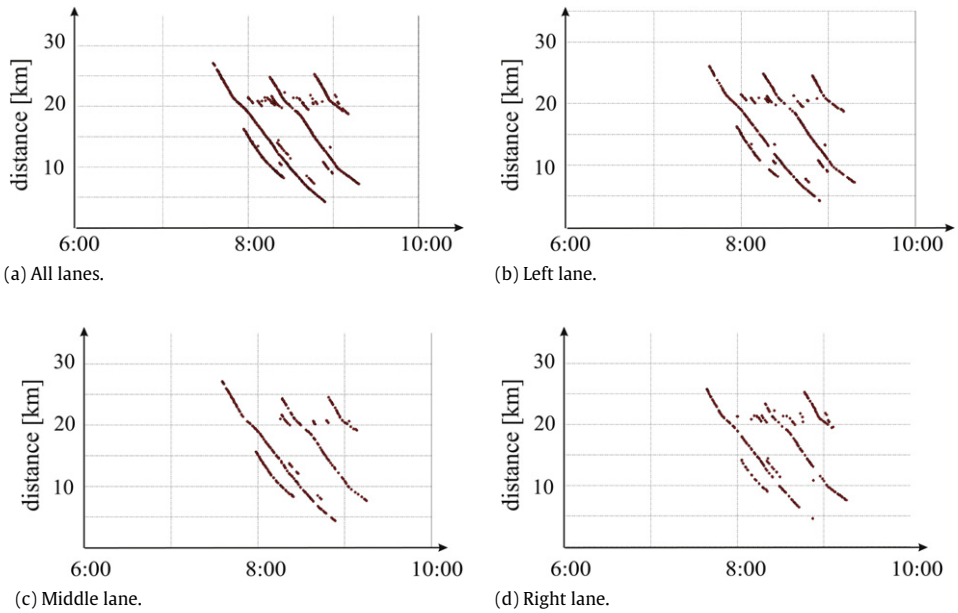

Fig. 17. Detection of upstream jam fronts ("jam warning messages") in different road lanes with $\eta = 5\%$ of probe vehicles: (a) All lanes. (b) Left lane. (c) Middle lane. (d) Right lane.

Therefore, a problem arises to find the transition points on vehicle trajectories that belong together and define the spatiotemporal structure of regions of synchronized flow and wide moving jams. The synchronized flow and wide moving jam phases show qualitatively different spatiotemporal empirical features [5]. Therefore, we apply the FOTO model for the reconstruction of synchronized flow and ASDA model for the reconstruction of wide moving jams for small η. Specific features of the FOTO and ASDA models for probe vehicle data based on empirical features of the different traffic phases are discussed in Appendix B.

Based on single vehicle data derived in simulations presented in Fig. 7(a) for $\eta = 100\%$, we have found transition points between different traffic phases and the reconstruction of regions of synchronized flow and wide moving jams with the models FOTO and ASDA for different small penetration rates of probe vehicles. Results of this analysis are presented in

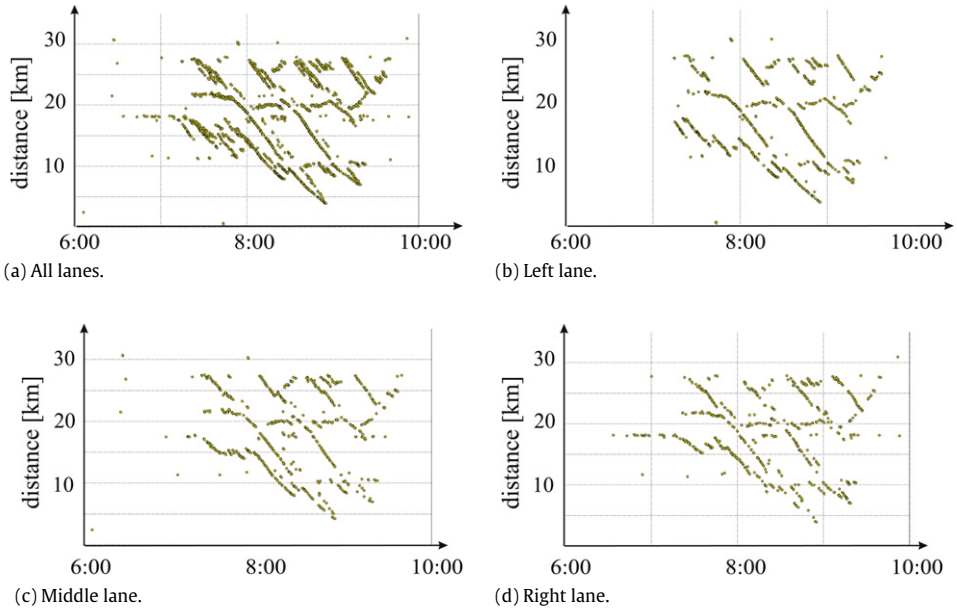

Fig. 18. Detection of F_S transitions in different road lanes with $\eta = 5\%$ of probe vehicles: (a) All lanes. (b) Left lane. (c) Middle lane. (d) Right lane.

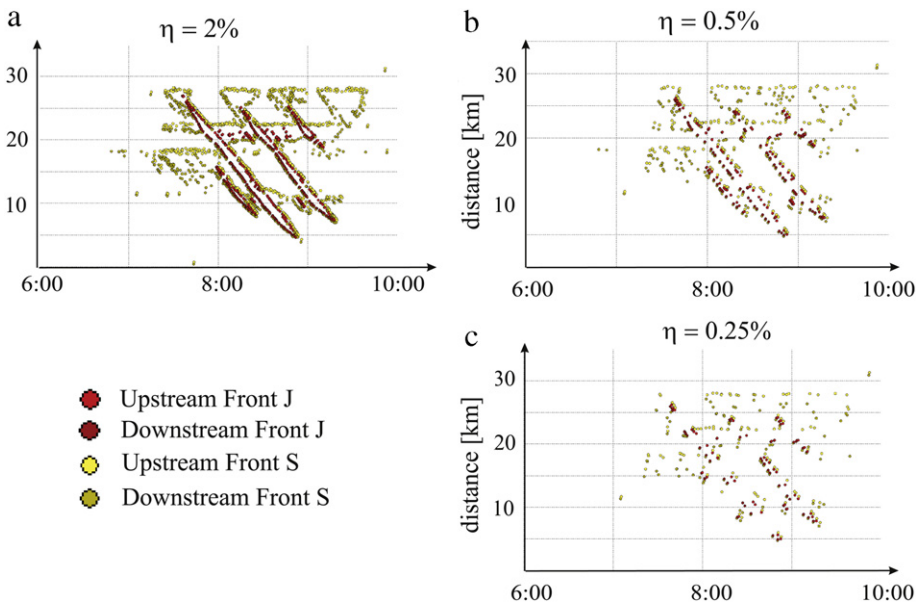

Fig. 19. Transitions points for different penetration rates of probe vehicles: (a) $\eta = 2\%$, (b) 0.5%, (c) 0.25%. Results of microscopic simulations.

Figs. 19 and 20, respectively. The obvious result of this analysis is that the overall quality of the pattern reconstruction decreases as the penetration rate of probe vehicles in total traffic flow decreases as well. A specific result is that with a decrease in the penetration rate of probe vehicles a higher reconstruction quality of wide moving jams is possible compared to regions of synchronized flow. This is because wide moving jams propagate while maintaining the mean velocity of the jam downstream front. Hence, a smaller amount of transitions points on trajectories of probe vehicles is sufficient to describe the structure of a wide moving jam with adequate quality.

To find how the quality of spatiotemporal pattern reconstruction depends on the distribution of probe vehicles within the traffic pattern shown in Fig. 7(a), 100 different random distributions of probe vehicles at each given η have been calculated. Finally, for these 100 realizations standard deviations of the hit, miss, and false alarm rates called quality indices have been found. We have found that with a decrease in the penetration rate η the hit rates for regions of synchronized flow suffer already at 0.5%, achieving a hit rate of only 54%, while the hit rates for wide moving are good down to 0.25%, where a hit rate

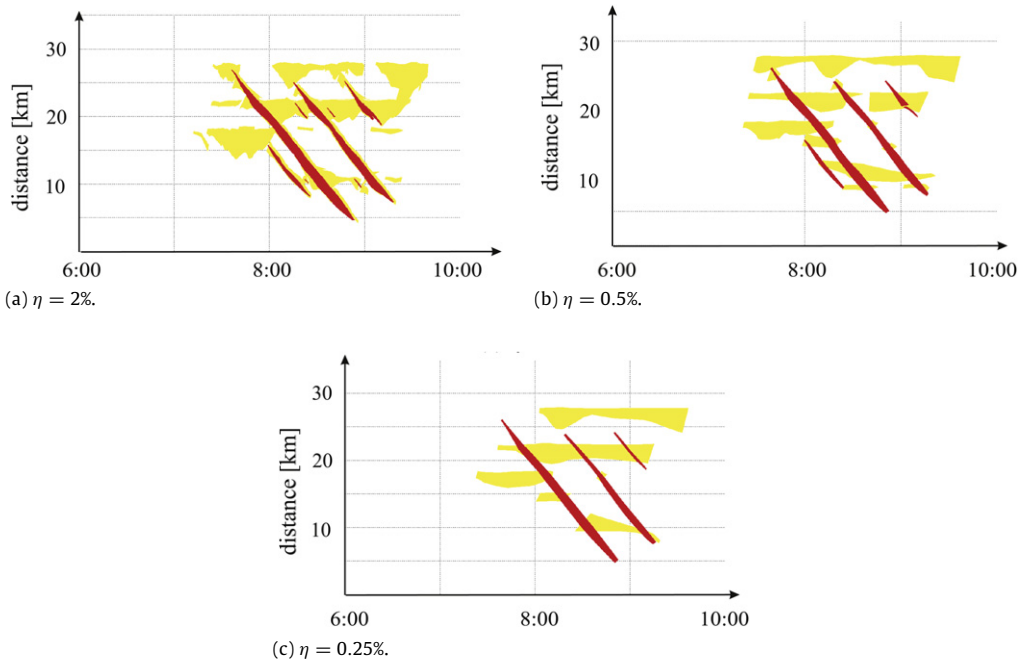

Fig. 20. Reconstruction of congested patterns with FOTO and ASDA models of Appendix B based on the simulated transition points shown in Fig. 19: (a) $\eta = 2\%$, (b) 0.5%, (c) 0.25%.

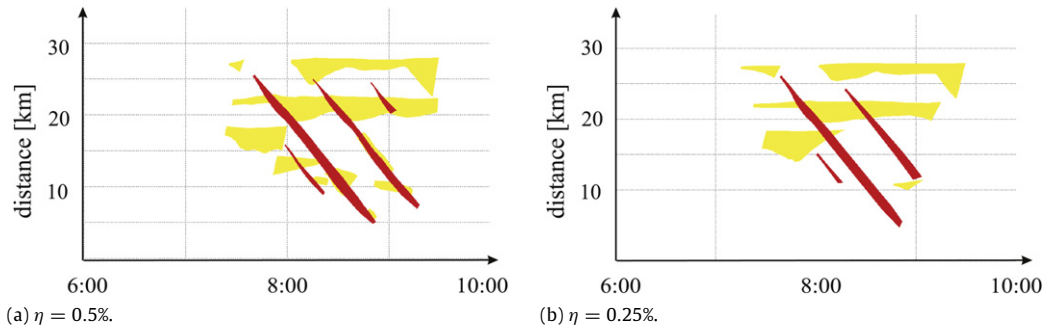

Fig. 21. Reconstruction of congested patterns with FOTO and ASDA models based on other realizations for random distributions of probe vehicles in comparison to those used in Fig. 19(b) and (c) for the associated penetration rates: (a) $\eta = 0.5\%$, (b) 0.25%.

of 63% is still achievable. However, at this penetration rate the hit rate for regions of synchronized flow is only 37% (Fig. 20(c)). The false alarm rates of wide moving jam and synchronized flow are comparable. This is because at small penetration rates of probe vehicles less congested regions are detected and, therefore, also less false detections occur. In addition, standard deviations of these quality indices increase with decreasing penetration rates of probe vehicles; therefore, a probe vehicle distribution within the pattern with $\eta = 0.25\%$ might be possible for which associated quality indices are almost the same as for a probe vehicle distribution with $\eta = 0.5\%$.

To illustrate the influence of different realizations of random distributions of probe vehicles within the pattern on the reconstruction of congested traffic patterns with the FOTO and ASDA models of Appendix B, in Fig. 21 we show the reconstructed pattern from other random distributions of probe vehicles than those used in Fig. 20(b, c). We can see that for the same η synchronized flow regions are slightly different in these realizations. In addition, the rightmost wide moving jam that can be seen in Fig. 20(c) for $\eta = 0.25\%$ is missing in another realization of random distribution of probe vehicles at $\eta = 0.25\%$ shown in Fig. 21(b).

7. Conclusions

1. The analysis of empirical probe vehicle data with three-phase theory allows us to explain, reconstruct, and predict the spatiotemporal picture of traffic breakdown and resulting congested patterns on multi-lane roads almost as precisely as

observed in other real data measured by road detectors. Based on the empirical study of TomTom probe vehicle data, we have shown that in accordance with three-phase theory (i) the occurrence of congested traffic, i.e., traffic breakdown is associated with an F $\rightarrow$ S transition; (ii) wide moving jams emerge spontaneously in synchronized flow (S $\rightarrow$ J transitions); (iii) after the F $\rightarrow$ S transition has occurred, the downstream front of the synchronized flow is usually fixed at some road location; (iv) in contrast with this synchronized flow front, the downstream front of a wide moving jam at which vehicles accelerate from the jam to another traffic phase propagates through the road while maintaining the mean velocity of the downstream jam front.

2. Based on empirical inflow and outflow rates measured by road detectors on a three-lane road section with on- and off-ramp bottlenecks, a stochastic three-phase model developed in the article can simulate both traffic breakdown at the bottlenecks and resulting complex spatiotemporal congested patterns very close both qualitatively and quantitatively to empirical data measurements made both with probe vehicle data and road detectors.
3. Physical features and limitations of simulations of complex empirical congested patterns are found. In particular, in different simulation realizations (runs) made at the same inflow and outflow rates but different initial conditions for model fluctuations we have found different time instants for traffic breakdown at the bottlenecks as well as a complex stochastic behavior of the emergence and dissolution of wide moving jams. These simulation results are in agreement with probabilistic features of empirical traffic breakdown and wide moving jam emergence found in observations of real traffic made during many years of data measurements [5] (see Sec. 2.4.10 in this book).
4. A simple model of traffic phase identification along a vehicle trajectory based on three-phase theory allows us to make a reliable generation of danger messages like traffic jam warning as well as to reconstruct many important features of spatiotemporal congested patterns already at the penetration rate 0.5% of probe vehicles randomly distributed in traffic flow.
5. When the penetration rate of probe vehicles randomly distributed in traffic flow achieves above 2% of all vehicles, a high quality reconstruction of almost the whole spatiotemporal traffic dynamics of synchronized flow and wide moving jams is possible.
6. The ASDA and FOTO models based on probe vehicle data are a useful practical instrument for the spatiotemporal reconstruction, tracking, and prediction of congested traffic patterns on highways, especially where no stationary road detection sites are available. The reconstruction of spatiotemporal congested patterns with the ASDA and FOTO models is already possible at a small penetration rate of probe vehicles about 0.5%, while still achieving a hit rate of 76% for wide moving jams and 54% for regions of synchronized flow.

Appendix A. Kerner–Klenov stochastic three-phase traffic flow model for three-lane road with on- and off-ramp bottlenecks

In this Appendix, the Kerner–Klenov stochastic three-phase traffic flow model for three-lane road with on- and off-ramp bottlenecks used in all simulations of the main text is presented and discussed.

A.1. Update rules of vehicle motion

We use a discrete version of the Kerner–Klenov stochastic microscopic three-phase traffic flow model [49]; a continuum version of this model has initially been developed in Ref. [48]. However, the following changes have been made in the model caused by features of real measured data: firstly, as mentioned above we have made a further model development to perform realistic traffic simulations on a three-lane road under consideration with on- and off-ramp bottlenecks (Fig. 6(a)). Secondly, in the measured data there are data of average speeds and flow rates separately for passenger and long vehicles. Thus, we simulate a heterogeneous traffic consisting of these two types of vehicles. Although all vehicles move with the same update rules of vehicle motion, some model functions and parameters in these rules are different; in particular, these two vehicle types exhibit different maximum speeds in free flow, different vehicle lengths, as well as different driver time delays in some driving situations. Finally, in contrast to the model versions of Refs. [48–51], in the model dependencies of free flow speed on the density found from measured data are used (Fig. A.1).

In the model, a small enough value of the discretization cell δx is used [49,50]. Consequently, the vehicle speed and acceleration (deceleration) discretization intervals are $\delta v = \delta x/\tau$ and $\delta a = \delta v/\tau$, respectively, where time step $\tau = 1$ s. Because in the discrete model version discretized (and dimensionless) speed and acceleration are used, which are measured respectively in the discretization values δv and δa, the value τ in all formulae below is assumed to be the dimensionless value $\tau = 1$. This leads to the following update rules of vehicle motion in the model:

$$v_{n+1} = \max(0, \min(v_{\text{free}}(g_n), \tilde{v}_{n+1} + \xi_n, v_n + a\tau, v_{s,n})), \tag{A.1}$$

$$x_{n+1} = x_n + v_{n+1}\tau, \tag{A.2}$$

$$\tilde{v}_{n+1} = \max(0, \min(v_{\text{free}}, v_{c,n}, v_{s,n})), \tag{A.3}$$

$$v_{c,n} = \begin{cases} v_n + \Delta_n & \text{at } g_n \le G_n \\ v_n + a_n\tau & \text{at } g_n > G_n, \end{cases} \tag{A.4}$$

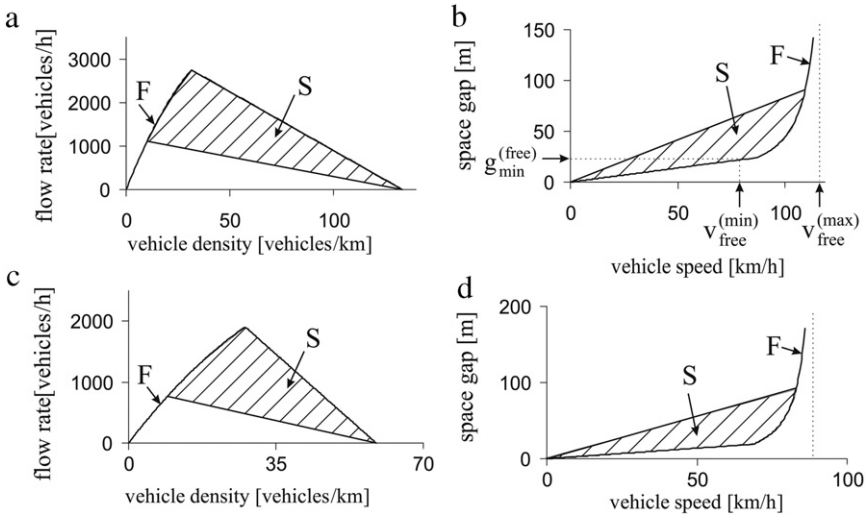

Fig. A.1. Model steady states for passenger vehicles (a, b) and long vehicles (c, d): (a, c) Steady states in the flow–density plane. (b, d) Steady states in the space–gap–speed plane. F - free flow. S - synchronized flow. In (b), $v_{free}^{(max)}$ and $v_{free}^{(min)}$ are the maximum and minimum free flow speed of passenger vehicles, $g_{min}^{(free)}$ is the minimum space gap in free flow related to the speed $v_{free}^{(max)}$.

where

$$\Delta_n = \max(-b_n\tau, \min(a_n\tau,\ v_{\ell,n} - v_n)), \tag{A.5}$$

$n = 0, 1, 2, \ldots$ is number of time steps, $\tilde{v}_n$ is the vehicle speed at time step n without speed fluctuations ξ_n, $v_{s,n}$ is a safe speed at time step n, $g_n = x_{\ell,n} - x_n - d$, the lower index ℓ marks variables related to the preceding vehicle, d is a vehicle length, G_n is a synchronization space gap, a is a maximum acceleration. With the exclusion of a function for the maximum speed in free flow $v_{free}(g_n)$, other model functions are the same for passenger and long vehicles. The maximum speed $v_{free}(g_n)$ is determined by formula:

$$v_{free}(g_n) = \max(v_{free}^{(min)}, v_{free}^{(max)}(1 + c_1 d/(g_n + d))^{-1}), \tag{A.6}$$

where $v_{free}^{(min)}$, $v_{free}^{(max)}$, and c_1 are constants that can be different for passenger and long vehicles. Explanations of the physics of vehicle motion rules in the model can be found in Sect. 16.3 of [5]. Model functions ξ_n, G_n, b_n, and $v_{s,n}$ are the same as those of Ref. [49,50]; therefore, these functions together with model parameters used for simulations are presented in Appendix A.5. In contrast with these known model functions [49,50], novel elements of the model are lane changing rules for a three-lane road as well as some features of on- and off-ramp bottlenecks on the three-lane road. A general feature of this model development presented below is that this can also be used for simulations of statistical physical features of traffic flow on other multi-lane roads with bottlenecks.

A.2. Lane changing rules on three-lane road

By the formulating of lane changing rules on a three-lane road, we use some ideas of the explicit simulation of vehicle over-acceleration through the use of lane changing to the faster lane of Sect. II.E of Ref. [49]. Lane changing rules from the right lane to the middle lane and from the middle lane to the left lane are as follows:

$$v_n^+ \geq v_{\ell,n} + \delta_1 \quad \text{and} \quad v_n \geq v_{\ell,n}. \tag{A.7}$$

Lane changing rules from the middle lane to the right lane and from the left lane to the middle lane are as follows:

$$v_n^+ > v_{\ell,n} + \delta_2 \quad \text{or} \quad v_n^+ > v_n + \delta_2, \tag{A.8}$$

where $\delta_1 > 0$ and $\delta_2 > 0$ are constants, $\delta_1 < \delta_2$ for personal vehicles and $\delta_1 > \delta_2$ for long vehicles; superscripts $+$ and $-$ in variables, parameters, and functions denote the preceding vehicle and the trailing vehicle in the "target" (neighboring) lane, respectively; the target lane is the lane into which the vehicle wants to change; the speed v_n^+ or the speed $v_{\ell,n}$ (A.7) and (A.8) is set to ∞ if the space gap g_n^+ or the space gap g_n exceeds a given look-ahead distance L_a, respectively.

When these lane changing rules are satisfied, a vehicle changes lane with probability p_c, if in addition one of the following sets of safety conditions for lane changing are satisfied. The first set of the safety conditions for lane changing is:

$$g_n^+ > \min(v_n\tau,\ G_n^+), \tag{A.9}$$

$$g_n^- > \min(v_n^-\tau,\ G_n^-), \tag{A.10}$$

where

$$G_n^+ = G(v_n, v_n^+), \tag{A.11}$$

$$G_n^- = G(v_n^-, v_n), \tag{A.12}$$

$G(u, w)$ is given by (A.47); after lane changing, the coordinate and speed of the vehicle are x_n and v_n, respectively.

When the safety conditions (A.11), (A.12) are not satisfied, then a vehicle can nevertheless change to a faster lane with the above-mentioned given probability p_c, if the following second set of safety conditions is satisfied: The space gap between two neighboring vehicles in the target lane satisfies the condition

$$x_n^+ - x_n^- - d^+ > g_{\text{target}}^{(\min)}, \tag{A.13}$$

where

$$g_{\text{target}}^{(\min)} = \lfloor \lambda v_n^+ + d \rfloor, \tag{A.14}$$

λ is constant; in addition to (A.13), the vehicle should pass the midpoint $x_n^{(\text{m})}$ between two neighboring vehicles in the target lane found from the formula

$$x_n^{(\text{m})} = \lfloor (x_n^+ + x_n^- + d - d^+)/2 \rfloor, \tag{A.15}$$

specifically, the following conditions should be satisfied

$$\begin{aligned} &x_{n-1} < x_{n-1}^{(\text{m})} \quad \text{and} \quad x_n \geq x_n^{(\text{m})} \\ &\text{or} \\ &x_{n-1} \geq x_{n-1}^{(\text{m})} \quad \text{and} \quad x_n < x_n^{(\text{m})}, \end{aligned} \tag{A.16}$$

$\lfloor z \rfloor$ denotes the integer part of a real number z. After lane changing, the coordinate of the vehicle is set to $x_n = x_n^{(\text{m})}$ and the vehicle speed v_n is set to $\hat{v}_n$:

$$\hat{v}_n = \min(v_n^+, v_n + \Delta v^{(1)}), \tag{A.17}$$

where $\Delta v^{(1)}$ is a constant.

It is assumed that if the speed in the right lane is high enough, long vehicles moving first in the middle lane are usually forced to change to the right lane, whereas long vehicles moving in the right lane keep the lane. The same situation occurs, when long vehicles moving first in the left lane are usually forced to change to the middle lane, whereas long vehicles moving in the middle lane do not change to the left lane. To simulate this effect, the following lane changing rules have been added to the incentive criteria (A.7) and (A.8). A long vehicle changes from the left lane to the middle lane or from the middle lane to the right lane even if the conditions (A.8) are not satisfied but the condition

$$v_n^+ > v_{\text{free, long}}^{(\max)} - \delta_0, \tag{A.18}$$

holds. Here $\delta_0 > 0$ is a constant $v_{\text{free, long}}^{(\max)}$ is the maximum speed for long vehicles. A long vehicle changes from the right lane to the middle lane or from the middle lane to the right lane only if the related condition

$$v_{\ell,n} \leq v_{\text{free, long}}^{(\max)} - \delta_0. \tag{A.19}$$

is satisfied together with (A.7). In both cases, the security rules should also be satisfied for lane changing.

Simulations show that these lane changing rules for a three-lane road allows us an explicit simulation of the over-acceleration effect through lane changing to a faster lane, even if no other mathematical formulations for over-acceleration are applied; specifically, in (A.37) for all simulations we have used

$$p_{\text{a}} = 0 \tag{A.20}$$

as applied for simulations in Refs. [49,49,51] for a two-lane road.

A.3. Models of on- and off-ramp bottlenecks on a three-lane road

There are five on-ramps and four off-ramps on the three-lane freeway section under consideration, which can act as effectual bottlenecks (Fig. 6(a)).

In the model of on-ramp bottlenecks, we assume that within a road section length L_{d} upstream of an on-ramp and within the on-ramp merging region L_{m} (Fig. A.2(a)), the personal vehicles moving in the right lane on the main road try to change to the middle lane, and the vehicles moving in the middle lane try to change to the left lane.

Similarly, in the model of off-ramp bottleneck we assume that within a road section length L_{d} upstream of an off-ramp and within the off-ramp merging region $L_{\text{c}} + L_{\text{m}}$ (Fig. A.2(b)) the vehicles that are not going to the off-ramp try to change from the right to the middle lane and from the middle to the left lane.

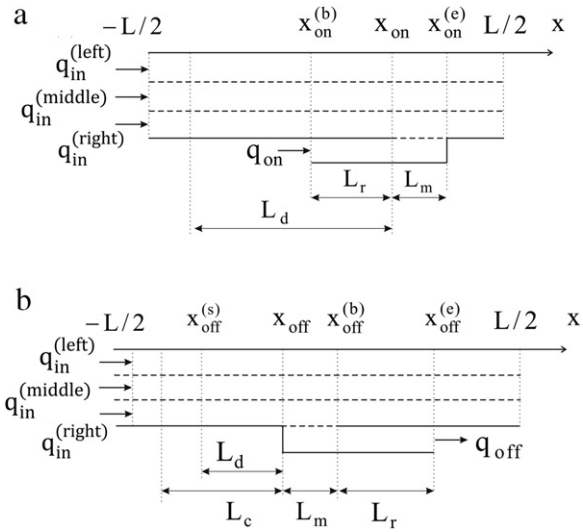

Fig. A.2. Models of on-ramp (a) and off-ramp (b) bottlenecks on three-lane road.

To simulate this effect, within the region

$$x_{\text{on}} - L_{\text{d}} \le x_n \le x_{\text{on}} + L_{\text{m}} \tag{A.21}$$

for on-ramp and within the region

$$x_{\text{off}} - L_{\text{d}} \le x_n \le x_{\text{off}} + L_{\text{m}} \tag{A.22}$$

for off-ramp and when the conditions (A.7), (A.9)–(A.16) are satisfied, the probability of lane changing is set to $p_{\text{c}} = 1$.

Vehicle merging occurs within the merging region L_{m} of the on-ramp bottleneck (Fig. A.2(a)) and within the merging region $L_{\text{c}} + L_{\text{m}}$ of the off-ramp bottleneck (Fig. A.2(b)) when the following safety conditions $(*)$ *or* $(**)$ are satisfied. The safety conditions $(*)$ are as follows:

$$g_n^+ > \hat{v}_n \tau \quad \text{and} \quad g_n^- > \min(\lambda_{\text{b},1} v_n^- \tau,\ G(v_n^-, \hat{v}_n)), \tag{A.23}$$

or

$$g_n^+ > \min(\lambda_{\text{b},1} \hat{v}_n \tau,\ G(\hat{v}_n, v_n^+)) \quad \text{and} \quad g_n^- > v_n^- \tau, \tag{A.24}$$

$$\hat{v}_n = \min(v_n^+, v_n + \Delta v_r^{(1)}), \tag{A.25}$$

$\Delta v_r^{(1)} > 0$ is constant, $\lambda_{\text{b},1} = c_{\text{b}} \lambda_{\text{b}}$, c_{b} is constant, λ_{b} can be a constant for some bottlenecks, for other bottlenecks λ_{b} can be chosen as a function of average gap $g_{\text{avr,n}}^{(\text{tag})}$ between N_{avr} subsequent vehicles ahead in the target lane:

$$g_{\text{avr,n}}^{(\text{tag})} = \frac{1}{N_{\text{avr}}} \sum_{i=1}^{i=N_{\text{avr}}} g_{i,n}^{(\text{tag})}, \tag{A.26}$$

where $g_{i,n}^{(\text{tag})}$ is a gap in front of the vehicle with index "i" in the target lane, the initial number $i = 1$ corresponds to the trailing vehicle in the target lane, the vehicle with index "i" is a preceding one for the vehicle with index "i-1".

As a function $\lambda_{\text{b}}(g_{\text{avr,n}}^{(\text{tag})})$, an increasing piece-linear function is used:

$$\lambda_{\text{b}}(g_{\text{avr,n}}^{(\text{tag})}) = \lambda_{\text{b}}^{(0)} + (\lambda_{\text{b}}^{(1)} - \lambda_{\text{b}}^{(0)}) \max(0, \min(1, (g_{\text{avr,n}}^{(\text{tag})} - g_1)/\Delta g_1)), \tag{A.27}$$

where $\lambda_{\text{b}}^{(0)} < \lambda_{\text{b}}^{(1)}, g_1, \Delta g_1$ are constants.

The safety condition $(**)$ is given by formula (A.13) in which

$$g_{\text{target}}^{(\text{min})} = \lfloor \lambda_{\text{b}} v_n^+ + d \rfloor, \tag{A.28}$$

λ_{b} is given by (A.27); in addition, the vehicle should pass the midpoint $x_n^{(\text{m})}$ (A.15) between two neighboring vehicles in the target lane, i.e., the conditions (A.16) should be satisfied.

Parameters after vehicle merging:

$$v_n = \hat{v}_n, \tag{A.29}$$

under the rule (∗) the vehicle coordinate x_n does not change, under the rule (∗∗):

$$x_n = x_n^{(\mathrm{m})}. \tag{A.30}$$

Speed adaptation before vehicle merging:

$$v_{\mathrm{c},n} = \begin{cases} v_n + \Delta_n^+ & \text{at } g_n^+ \le G(v_n, \hat{v}_n^+) \\ v_n + a_n\tau & \text{at } g_n^+ > G(v_n, \hat{v}_n^+) \end{cases} \tag{A.31}$$

$$\Delta_n^+ = \max(-b_n\tau, \min(a_n\tau,\ \hat{v}_n^+ - v_n)), \tag{A.32}$$

$$\hat{v}_n^+ = \max(0, \min(v_{\mathrm{free}},\ v_n^+ + \Delta v_r^{(2)})), \tag{A.33}$$

$\Delta v_r^{(2)}$ is constant.

The same rules for vehicle merging are used in models of an on-ramp bottleneck (Fig. A.2(a)) and an off-ramp bottleneck (Fig. A.2(b)), i.e., when a vehicle merges from the on-ramp onto the main road or a vehicle leaves the main road to the off-ramp.

The safe speed $v_{\mathrm{s},n}$ in (A.3) for the vehicle that is the closest one to the end of merging region is chosen in the form

$$v_{\mathrm{s},n} = \lfloor v^{(\mathrm{safe})}(x_{\mathrm{on}}^{(\mathrm{e})} - x_n)\rfloor, \tag{A.34}$$

for on-ramp bottlenecks

$$v_{\mathrm{s},n} = \min(v_n^{(\mathrm{safe})}, g_n/\tau + v_\ell^{(\mathrm{a})}, \lfloor v^{(\mathrm{safe})}(x_{\mathrm{off}}^{(\mathrm{e})} - x_n - L_{\mathrm{s}})\rfloor), \tag{A.35}$$

for off-ramp bottlenecks, where L_{s} is a constant.

A.4. Boundary conditions

As in real traffic, in a model of three-lane road with on-ramp and off-ramp bottlenecks (these bottlenecks are within road intersections denoted by I1–I3 in Fig. 6(a)) vehicles appear at the upstream road boundary $x = 0$ of the main road and from the on-ramps; vehicles leave the main road to the off-ramps and at the downstream road boundary $x = 30.5$ km. In this open traffic process, all traffic variables on the main road within road locations $0 < x < 30.5$ km result *only* from traffic modeling at the following boundary conditions: (i) The time-dependence of the flow rate at the upstream road boundary $x = 0$ is taken from measurements at the detectors located at $x = 0$ (Fig. 6). (ii) The time-dependences of the on-ramp inflow rates are taken from measurements of these flow rates at the detectors located at the associated on-ramps (Fig. 6). (iii) The time-dependences of the flow rates of vehicles leaving the main road to the off-ramps are taken from measurements of these flow rates at the detectors located at the associated off-ramps (Fig. 6). (iv) At the downstream model boundary $x = 30.5$ km, free flow conditions for vehicles leaving the road section are given.

None of the flow rates (or vehicle speeds or else other traffic variables) measured by the detectors on the main road within the simulation road section $0 < x < 30.5$ km are used in simulations. Moreover, we use in the boundary conditions of simulations the flow rates measured separately for personal and long vehicles (Fig. 6(b)). In other words, we simulate the *self-development of traffic* on the main three-lane road section with the same locations of on- and off-ramps and the same associated flow rates to the on-ramps and flow rates to the off-ramps as those measured in real traffic within the road locations $0 < x < 30.5$ km, i.e., between the detectors located at $x = 0$ and $x = 30$ km on the main road of the section of the freeway A5-South. Note that initial conditions in simulations are taken as described in Sec. 13.3 of the book [5].

A frequently asked question in the literature is as follows: what is qualitatively different and probably the same in the Kerner–Klenov three-phase traffic model in comparison with well-known two-phase microscopic traffic flow models [1,7] criticized in the Section 1? The responses to this question are as follows:

Main qualitative differences:

1. In the Kerner–Klenov model, a hypothesis of three-phase traffic theory about the existence of a Z-shape density function for probability of vehicle passing (see Fig. 5.7(b) of [5] or Figs. 3.6 and 3.7 of [6]) is incorporated. In contrast with two-phase traffic flow models [1,7], this feature of three-phase theory incorporated in the Kerner–Klenov model allows us to simulate all fundamental empirical features of traffic breakdown at a bottleneck (see Chap. 3 of [6]).
2. In the Kerner–Klenov model, the fundamental hypothesis of three-phase traffic theory is used: Hypothetical steady states of synchronized flow cover a two-dimensional (2D) region in the flow-density plane (Fig. A.1(a)), i.e., no fundamental diagram is used for the steady states. The physics of the fundamental hypothesis has been discussed in detail in a recent article [51]. In application of the model version used for simulations of the heterogeneous traffic, there are two different 2D-regions in the flow-density plane for passenger vehicles (Fig. A.1(a)) and long vehicles (Fig. A.1(c)), respectively.

Main similarities:

The Kerner–Klenov model incorporates many pertinent ideas about simulations of a variety of driver time delays in different driving situations of earlier traffic flow models in the framework of the fundamental diagram hypothesis introduced

by Herman et al. [52], Gazis et al. [53], Newell [54], Nagel, Schreckenberg, Schadschneider, and co-workers [55,56], Bando, Sugiyama, and colleagues [57] and many other groups. The Kerner–Klenov model uses a formulation for a safe speed introduced by Gipps [59] and Krauß et al. [58].

A.5. Functions for driver behavioral characteristics incorporated in the Kerner–Klenov three-phase model

Here, model functions ξ_n, G_n, b_n, and $v_{s,n}$ used in the Kerner–Klenov model (A.1)–(A.5) are presented.

A.5.1. Model speed fluctuations

Random deceleration and acceleration ξ_n in (A.1) are applied depending on whether the vehicle decelerates or accelerates, or else maintains its speed [49]:

$$\xi_n = \begin{cases} \xi_a & \text{if } S_{n+1} = 1 \\ \xi_b & \text{if } S_{n+1} = -1 \\ \xi^{(0)} & \text{if } S_{n+1} = 0, \end{cases} \tag{A.36}$$

where

$$\xi_a = a^{(a)}(v_n)\tau\Theta(p_a - r), \tag{A.37}$$

$$\xi_b = a^{(b)}(v_n)\tau\Theta(p_b - r), \tag{A.38}$$

$$\xi^{(0)} = a^{(0)}\tau \begin{cases} -1 & \text{if } r < p^{(0)} \\ 1 & \text{if } p^{(0)} \le r < 2p^{(0)} \quad \text{and} \quad v_n > 0 \\ 0 & \text{otherwise}, \end{cases} \tag{A.39}$$

where p_a and p_b are respectively probabilities of random acceleration and deceleration; $r = \text{rand}(0, 1)$, $\Theta(z) = 0$ at $z < 0$ and $\Theta(z) = 1$ at $z \ge 0$. S in (A.36) denotes the state of motion ($S_{n+1} = -1$ represents deceleration, $S_{n+1} = 1$ acceleration, and $S_{n+1} = 0$ motion at constant speed):

$$S_{n+1} = \begin{cases} -1 & \text{if } \tilde{v}_{n+1} < v_n \\ 1 & \text{if } \tilde{v}_{n+1} > v_n \\ 0 & \text{if } \tilde{v}_{n+1} = v_n, \end{cases} \tag{A.40}$$

$p^{(0)}$ and $a^{(0)} \le a$ are constants. Thus in contrast with the continuum model of Ref. [8,48], in the discrete model version used in this article speed fluctuations appear also in an initial homogeneous traffic flow.

A.5.2. Stochastic driver time delay in acceleration and deceleration

Driver time delays in acceleration and deceleration are simulated as collective effects through the use of a random value of vehicle acceleration

$$a_n = a\Theta(P_0 - r_1) \tag{A.41}$$

and deceleration

$$b_n = a\Theta(P_1 - r_1), \tag{A.42}$$

where $r_1 = \text{rand}(0, 1)$, P_0 and P_1 are respectively probabilities of random acceleration and deceleration

$$P_0 = \begin{cases} p_0(v_n) & \text{if } S_n \ne 1 \\ 1 & \text{if } S_n = 1, \end{cases} \tag{A.43}$$

$$P_1 = \begin{cases} p_1 & \text{if } S_n \ne -1 \\ p_2(v_n) & \text{if } S_n = -1, \end{cases} \tag{A.44}$$

where p_1 is constant. To simulate the well-known slow-to-start rule [56], i.e., that the mean time delay in vehicle acceleration

$$\tau_{\text{del}}^{(a)}(v_n) = \frac{\tau}{p_0(v_n)} \tag{A.45}$$

is longer at the speed $v_n = 0$ than at $v_n > 0$, probability p_0 in (A.43) depends on the speed (see Table below).

A.5.3. Synchronization gap G_n

The synchronization space gap G_n depends on the vehicle speed v_n and on the speed of the preceding vehicle $v_{\ell,n}$

$$G_n = G(v_n, v_{\ell,n}), \tag{A.46}$$

where the function $G(u, w)$ is chosen as

$$G(u, w) = \max(0, \lfloor k\tau u + a^{-1}u(u - w)\rfloor), \tag{A.47}$$

Table A.1
Model parameters used for simulations of traffic flow on three-lane road.

Parameters for vehicle motion in road lane: $\tau = \tau_{\rm safe} = 1$ s, $d = 7.5$ m$/\delta x$ for personal vehicles, $d = 17$ m$/\delta x$ for long vehicles, $\delta x = 0.01$ m, $v_{\rm free}^{\rm (max)} = 33.33$ ms$^{-1}/\delta v$, $v_{\rm free,long}^{\rm (max)} = 25$ ms$^{-1}/\delta v$, $v_{\rm free}^{\rm (m)} = 15$ ms$^{-1}/\delta v$, $c_1 = 1.4$ for personal vehicles, $c_1 = 0.6$ for long vehicles, $b = 1$ ms$^{-2}/\delta a$, $\delta v = 0.01$ ms^{-1}, $\delta a = 0.01$ ms^{-2}, $k = 3$, $p_1 = 0.3$, $p_b = 0.15$, $p^{(0)} = 0.005$, $p_2(v_n) = 0.48 + 0.32\Theta(v_n - v_{21})$, $p_0(v_n) = 0.52 + 0.23\min(1, v_n/v_{01})$ for personal vehicles and $p_0(v_n) = 0.33 + 0.37\min(1, v_n/v_{01})$ for long vehicles, $v_{01} = 10$ ms$^{-1}/\delta v$, $v_{21} = 15$ ms$^{-1}/\delta v$, $a = 0.5$ ms$^{-2}/\delta a$. $a^{\rm (b)}(v_n) = 0.2a + 0.8a\max(0, \min(1, (v_{22} - v_n)/\Delta v_{22}))$, $a^{(0)} = 0.2a$, $a^{\rm (a)} = 0$, $v_{22} = 12.5$ ms$^{-1}/\delta v$, $\Delta v_{22} = 2.778$ ms$^{-1}/\delta v$.
Lane changing parameters (model of over-acceleration): $\delta_1 = 1$ ms$^{-1}/\delta v$ and $\delta_2 = 3.5$ ms$^{-1}/\delta v$ for passenger vehicles, $\delta_1 = 3.5$ ms$^{-1}/\delta v$ and $\delta_2 = 1$ ms$^{-1}/\delta v$ for long vehicles, $\delta_0 = 6$ ms$^{-1}/\delta v$, $L_{\rm a} = 150$ m$/\delta x$, $p_{\rm c} = 0.2$, $\lambda = 0.8$, $\Delta v^{(1)} = 2$ ms$^{-1}/\delta v$.

a is the maximum acceleration, $k > 1$ is constant, $\lfloor z \rfloor$ denotes the integer part of a real number z, because only integer values of the gap in units of δx are used in the discrete model under consideration.

A.5.4. Safe speed $v_{{\rm s},n}$

The safe speed $v_{{\rm s},n}$ in (A.3) is chosen in the form

$$v_{{\rm s},n} = \min(v_n^{\rm (safe)}, g_n/\tau + v_\ell^{\rm (a)}), \tag{A.48}$$

where $v_\ell^{\rm (a)}$ is an "anticipation" speed of the preceding vehicle at the next time step considered below, the safe speed $v_n^{\rm (safe)} = \lfloor v^{\rm (safe)}(g_n, v_{\ell,n}) \rfloor$ in (A.48) is taken the same as that in the Krauß's model [58], which is a solution of the Gipps's equation [59]

$$v^{\rm (safe)}\tau_{\rm safe} + X_{\rm d}(v^{\rm (safe)}) = g_n + X_{\rm d}(v_{\ell,{\rm n}}), \tag{A.49}$$

where $\tau_{\rm safe}$ is a safe time gap,

$$X_{\rm d}(u) = b\tau^2\left(\alpha\beta + \frac{\alpha(\alpha-1)}{2}\right) \tag{A.50}$$

is the distance traveled by the vehicle with an initial speed u at a time-independent deceleration b until it comes to a stop, $\alpha = \lfloor u/b\tau \rfloor$ and $\beta = u/b\tau - \alpha$ are the integer and the fractional part of $u/b\tau$ respectively, b is measured in units of δa. When $\tau_{\rm safe} = \tau$, from (A.49), (A.50) we get [58]:

$$v^{\rm (safe)}(g_n, v_{\ell,n}) = b\tau(\alpha_{\rm safe} + \beta_{\rm safe}), \tag{A.51}$$

where

$$\alpha_{\rm safe} = \left\lfloor \sqrt{2\frac{X_{\rm d}(v_{\ell,n}) + g_n}{b\tau^2} + \frac{1}{4}} - \frac{1}{2} \right\rfloor, \tag{A.52}$$

$$\beta_{\rm safe} = \frac{X_{\rm d}(v_{\ell,n}) + g_n}{(\alpha_{\rm safe}+1)b\tau^2} - \frac{\alpha_{\rm safe}}{2}. \tag{A.53}$$

The anticipation speed of the preceding vehicle at the next time step is chosen as

$$v_\ell^{\rm (a)} = \max(0, \min(v_{\ell,n}^{\rm (safe)},\ v_{\ell,n},\ g_{\ell,n}/\tau) - a\tau), \tag{A.54}$$

where $v_{\ell,n}^{\rm (safe)}$ is the safe speed for the preceding vehicle that is found as the safe speed of the vehicle $v_n^{\rm (safe)}$ (see formulae (A.51)–(A.53)), $g_{\ell,n}$ is the space gap in the front of the preceding vehicle. Model parameters and parameters of bottleneck models used in simulations are given in Tables A.1 and A.2, respectively.

Table A.2
Parameters of bottleneck models on three-lane road.

$\lambda_b = 0.75$ for all bottlenecks except with
off-ramps at the middle and the downstream bottlenecks,
for the latter bottlenecks λ_b is given by formulae (A.27)
where $g_1 = 20$ m/δx, $\Delta g_1 = 20$ m/δx,
$\lambda_b^{(0)} = 0.72$, $\lambda_b^{(1)} = 0.8$ for the off-ramp at the middle bottleneck,
$\lambda_b^{(0)} = 0.65$, $\lambda_b^{(1)} = 0.8$ for the off-ramp at the downstream bottleneck,
$\lambda_b = 0.6$ for long vehicles at all bottlenecks,
$\lambda_b = 0.65$ for all off-ramp lanes,
$c_b = 0.5$, $N_{avr} = 10$,
$L_c^{(off)}$ for passenger vehicles:
for the off-ramp at the downstream bottleneck:
$L_c^{(off)} = 0.3$ km/δx in the middle lane, $L_c^{(off)} = 0.6$ km/δx in the left lane,
for the off-ramp at the middle and the upstream bottlenecks:
$L_c^{(off)} = 0.5$ km/δx in the middle lane, $L_c^{(off)} = 1.0$ km/δx in the left lane,
for long vehicles and for all bottlenecks:
$L_c^{(off)} = 1.0$ km/δx in the middle lane,
$L_c^{(off)} = 2.0$ km/δx in the left lane,
$v_{free\ off} = 23.6$ ms^{-1}/δv, $L_d = 0.5$ km/δx,
$\Delta v_r^{(2)} = 5$ ms^{-1}/δv for on-ramp bottlenecks,
$\Delta v_r^{(2)} = 10$ ms^{-1}/δv for off-ramp bottlenecks, $\Delta v_r^{(1)} = 10$ ms^{-1}/δv,
$L_s = 0.1$ km/δx in the left lane, $L_s = 0.05$ km/δx in the middle lane,
$L_s = 0$ in the right lane, $L_r = 0.2$ km/δx for on-ramps and
$L_r = 0.1$ km/δx for off-ramps,
values L_m are taken from road infrastructure
for different on-ramps $L_{m,\ on\ i}$, $i = 1, 2, \ldots, 5$
are, respectively, 281, 300, 300, 415, 250 m
and for different off-ramps $L_{m,off\ j}$, $j = 1, 2, 3, 4$ are 210, 273, 2150, 1500 m.

Appendix B. Spatiotemporal reconstruction of traffic congestion with single vehicle data

In this Appendix, FOTO and ASDA models are considered, which are used in the main text for the spatiotemporal reconstruction of traffic congestion based on probe vehicles randomly distributed in traffic flow.

B.1. Tracking of synchronized flow: FOTO method for probe vehicle data

General empirical features of synchronized flow (the downstream front of synchronized flow is usually fixed at a highway bottleneck, whereas the upstream front can propagate either upstream or downstream [5,60]) are used in the FOTO model as follows (Fig. B.1):

1. The FOTO model distinguishes transition points on trajectories of probe vehicles, which are associated with the F_S and S_F transitions. Transition points on trajectories of probe vehicles driving one after another and which are associated with the same type of phase transition (special circles that label F_S transitions in Fig. B.1(a)) are considered to belong also to the same region of synchronized flow, if the temporal distance Δt between these points is shorter than some given maximum temporal distance Δt_{max} and the spatial distance Δd between these points does not exceed some given maximum spatial distance Δd_{max}. In a real world system, the error inherent to the measurement system is also taken into account. Hence, an error offset is added to both Δt_{max} and Δd_{max}. If the temporal and spatial conditions are satisfied, i.e., $\Delta t \le \Delta t_{max}$ and $\Delta d \le \Delta d_{max}$, then transition points are considered to belong to the same front of synchronized flow (Fig. B.1(b)).
2. If there are already two or more transition points assigned to a specific front of synchronized flow (F_S transitions in Fig. B.1(c)), then the following procedure is used to determine whether a point on a trajectory of the next probe vehicle associated with the same type of transition point belongs to the already existing front of synchronized flow or not. In order to approximate the front velocity, a linear regression of the latest transition points on this front is applied (dashed line in Fig. B.1(c)). A region in time-space plane around this linear regression is established whose size along the time axis is equal to Δt_{max} and along the direction axis is equal to $\Delta d_{max}^{(1)}$ and $\Delta d_{max}^{(2)}$, respectively at the beginning and end of the region (region bounded by dotted lines in Fig. B.1(c)). If a transition point for the next probe vehicle (of the same type as the transition point of a former probe vehicle) is within this region, then this transition point belongs to the front (point A in Fig. B.1(c)) and is added to the front of the same region of synchronized flow. Otherwise, the point does not belong to the same region of synchronized flow (points B and C in Fig. B.1(c)). In this case, a front of a new region of synchronized flow is established.

The application of the FOTO model is qualitatively illustrated in Fig. B.2. Firstly, we assume that on trajectories of two probe vehicles following each other the phase transitions points from free flow to synchronized flow (transition) have been identified (Fig. B.2(a)). If the temporal and spatial distances between these points satisfy the conditions and as this is the case in Fig. B.2(a), then the FOTO model assigns these points to the same upstream front of a region of synchronized flow

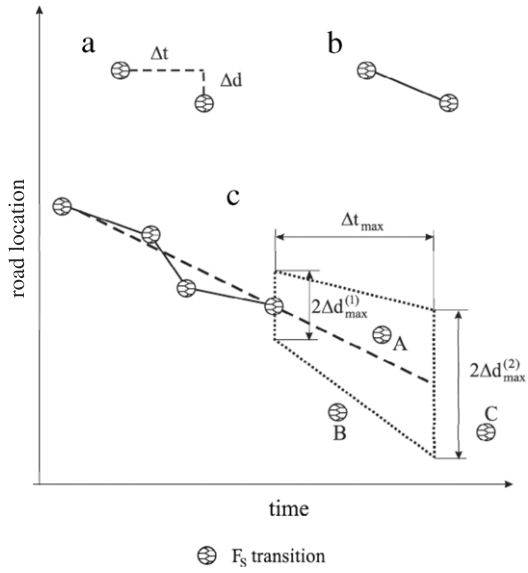

Fig. B.1. Qualitative explanation of the FOTO model for the reconstruction of synchronized flow. $\Delta t_{\max}$, $\Delta d_{\max}$, $\Delta d^{(1)}_{\max}$ and $\Delta d^{(2)}_{\max}$ are parameters associated with empirical characteristics of synchronized flow.

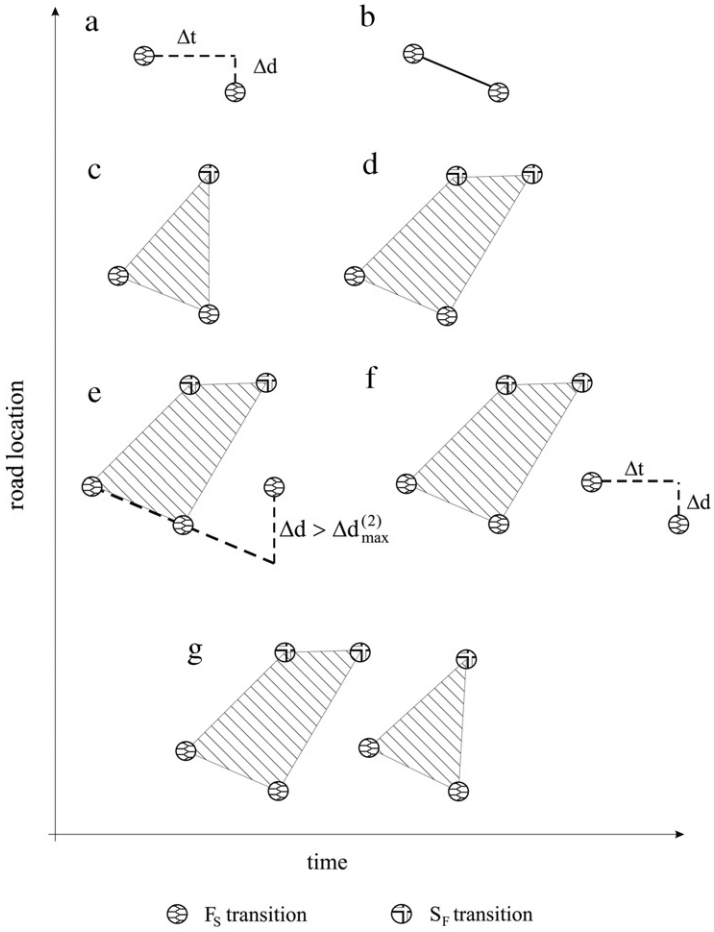

Fig. B.2. Qualitative illustration of the application of the FOTO model for the reconstruction of regions of synchronized flow.

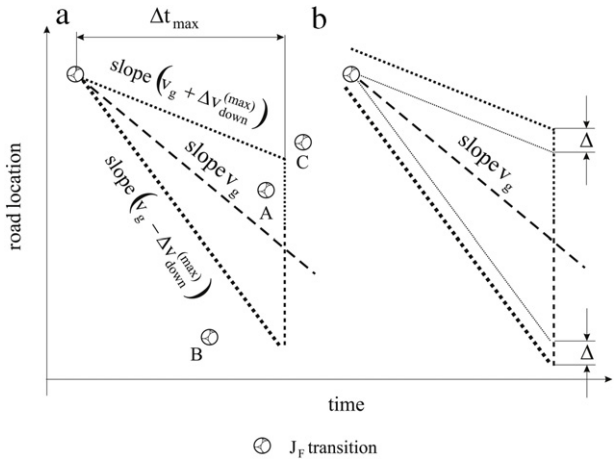

Fig. B.3. Qualitative explanation of the tracking of the downstream jam front with the ASDA model for probe vehicle data in an ideal case (a) and in a practical case, when measurement errors are taken into account (b).

(Fig. B.2(b)). At this time instant another transition point is detected on the trajectory of the first of these two vehicles. This transition point is associated with a transition, i.e., this point is related to the downstream front of the region of synchronized flow. Now the FOTO model creates a region of synchronized flow between these three points (Fig. B.2(c)). After some time another transition point associated with transition that resides on the downstream synchronized flow front is detected on the trajectory of the second of these two probe vehicles. Therefore, the FOTO model extends the downstream front with the transition point to create a greater region of synchronized flow between the four points (Fig. B.2(d)).

Later, another transition point associated with a F_S transition appears on the trajectory of a probe vehicle that follows the two probe vehicles mentioned above (Fig. B.2(e)). However, this transition point does not satisfy the condition $\Delta d \leq \Delta d^{(2)}_{\max}$. For this reason, the FOTO model recognizes this transition point as the beginning of the upstream front of a new region of synchronized flow. Based on data of the following probe vehicles, the FOTO model continues with the assignment of transition points to matching fronts by applying the algorithm described above (Fig. B.2(f, g)).

B.2. Tracking of wide moving jams: ASDA method for probe vehicle data

General empirical features of wide moving jams (a wide moving jam propagates upstream as a stable spatiotemporal congested structure through any other traffic phases or highway bottlenecks while maintaining the mean velocity v_g of the jam downstream front [5]) are used in the ASDA model as follows (Fig. B.3):

1. The ASDA model distinguishes transition points along trajectories of probe vehicles, which are associated with the wide moving jam phase.
2. *Tracking of the upstream jam front*: An upstream front of a wide moving jam corresponds to transition points on trajectories of probe vehicles associated with either F_J transition or S_J transition. After such a first transition point on a trajectory of a probe vehicle is found, the ASDA model builds a spatiotemporal region in the space–time plane exactly as that has been shown and explained in Fig. B.1 for the upstream front of synchronized flow. The only difference is here that the parameters $\Delta t_{\max}$, $\Delta d_{\max}$, $\Delta d^{(1)}_{\max}$ and $\Delta d^{(2)}_{\max}$ of this tracking of the upstream jam front in the ASDA model are different from those used in the FOTO model.
3. *Tracking of the downstream jam front*: A downstream front of a wide moving jam corresponds to transition points on trajectories of probe vehicles associated with either a J_F transition or J_S transition. After such a first transition point on a trajectory of a probe vehicle is found, the ASDA model builds a spatiotemporal region in the space–time plane with boundaries that are given by lines with slopes $v_g - \Delta v^{(\max)}_{\text{down}}$ and $v_g + \Delta v^{(\max)}_{\text{down}}$, respectively, where $\Delta v^{(\max)}_{\text{down}} > 0$; the size of this region along the time axis is equal to a maximum temporal distance $\Delta t_{\max}$ (Fig. B.3(a)). Here, v_g is the characteristic velocity of the propagation of the downstream jam front discussed above and $\Delta v^{(\max)}_{\text{down}}$, $\Delta t_{\max}$ are parameters of the ASDA model. The current value of v_g is approximated using a linear regression on the latest transition points for the downstream jam front. If the front consists of only one point (as this is shown in Fig. B.3(a)), a default value v_g is used (for example, $v_g = -15$ km/h). The spatiotemporal region bounded by the maximum temporal distance $\Delta t_{\max}$ and lines with slopes $v_g - \Delta v^{(\max)}_{\text{down}}$ and $v_g + \Delta v^{(\max)}_{\text{down}}$ is used as follows for the tracking of the downstream jam front. Two transition points on trajectories of probe vehicles following after each other and which are associated with the same transition type (J_F transitions labeled by special circles in Fig. B.3(a)) are considered to belong also to the downstream front of the same wide moving jam, if the temporal distance Δt between these transition points is shorter than $\Delta t_{\max}$ and if the deviation Δv_{down} of the slope of the line between these two points in the space–time plane from the slope v_g satisfies the condition

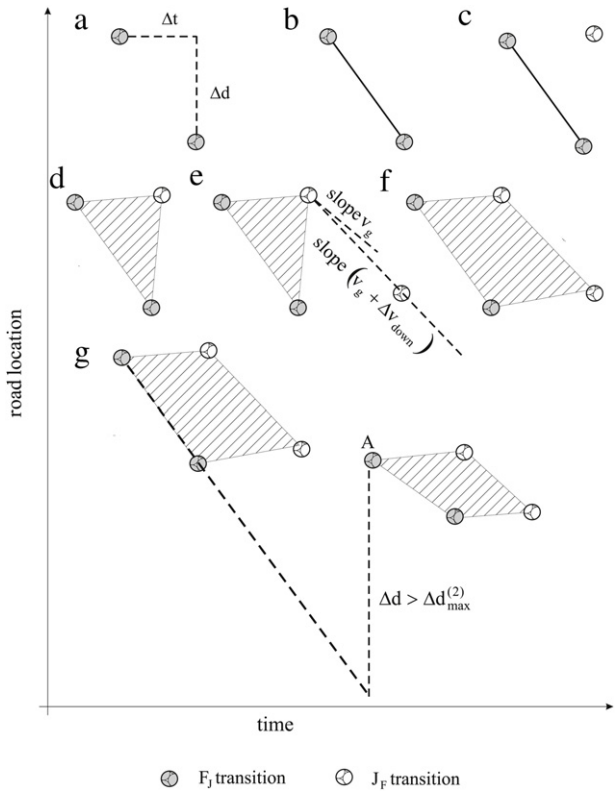

Fig. B.4. Qualitative illustration of the application of the ASDA model for the reconstruction and tracking of wide moving jams.

$|\Delta v_{\text{down}}| \leq \Delta v_{\text{down}}^{(\max)}$ (point A in Fig. 6(a)). Otherwise, the transition point is not associated with the same front of a wide moving jam (points B and C in Fig. B.3(a)). Both terms $v_g - \Delta v_{\text{down}}^{(\max)}$ and $v_g + \Delta v_{\text{down}}^{(\max)}$ in Fig. B.3(a) represent ideal cases without measurement errors. Hence, in a real world system the measurement error is also taken into account by adding error offsets Δ (Fig. B.3(b)). A choice of the v_g, $\Delta v_{\text{down}}^{(\max)}$, $\Delta t_{\max}$, and Δ (Fig. B.3) in the ASDA model is associated with empirical characteristics of wide moving jams; in particular, the choice of $\Delta v_{\text{down}}^{(\max)}$ is associated with a possible change in the percentage of long vehicles in traffic flow, weather, or other traffic parameters over time that can influence the current velocity of the downstream jam front considerably.

4. When a wide moving jam reconstructed by the ASDA model overlaps a region of synchronized flow reconstructed by the FOTO model, the wide moving jam has priority over the region of synchronized flow.

The application of the ASDA model is qualitatively illustrated in Fig. B.4. We assume that on trajectories of two probe vehicles following each other the transitions points from free flow to a wide moving jam (F_J transition) have been identified (Fig. B.4(a)). If the temporal Δt and spatial distances Δd between these points satisfy the conditions $\Delta t \leq \Delta t_{\max}$ and $\Delta d \leq \Delta d_{\max}$ as this is the case in Fig. B.4(a), then the ASDA model assigns these points to the same upstream front of a wide moving jam (Fig. B.4(b)). Then another transition point associated with a J_F transition is detected on the trajectory of the first of these two probe vehicles. Hence, this point is assigned to the downstream front of the wide moving jam (Fig. B.4(c)). In this case the ASDA model creates a region of the traffic phase J between these three points (Fig. B.4(d)). After some time, a transition point associated with a F_J transition that resides on the downstream jam front is also detected on the trajectory of the second of these two probe vehicles (Fig. B.4(e)). This transition point satisfies the conditions $|\Delta v_{\text{down}}| \leq \Delta v_{\text{down}}^{(\max)}$ and $\Delta t \leq \Delta t_{\max}$. For this reason, the ASDA model assigns this point to the downstream front to build a greater region of the traffic phase J between the four transition points (Fig. B.4(f)).

Some time later, a transition point (labeled by point A in Fig. B.4(g)) associated with a F_J transition appears on a trajectory of a probe vehicle that follows the two probe vehicles discussed above. However, this transition point does not satisfy the condition $\Delta d \leq \Delta d_{\max}$. For this reason, the ASDA model recognizes this transition point as part of the upstream front of a new wide moving jam. Based on data of the following probe vehicles, the ASDA model continues the assignment of transition points to jam fronts by applying the algorithm described above.

Note that an analysis of the quality of spatiotemporal pattern reconstruction with the FOTO and ASDA models for probe vehicle data considered in Ref. [61] shows a high performance of these models. In particular, at $\eta = 2\%$ of probe vehicles

randomly distributed in traffic flow, the false alarm for synchronized flow and wide moving jams have been only 0.14 and 0.11, respectively.

Appendix C. Spatiotemporal reconstruction of traffic congestion based on road detector measurements

In this Appendix we consider methods used in the main text for the spatiotemporal reconstruction of traffic dynamics between road detectors at which traffic variables are measured.

C.1. ASDA and FOTO methods for on-line spatiotemporal reconstruction of traffic congestion

The FOTO and ASDA models for automatic recognition and tracking of spatiotemporal congested traffic patterns have been introduced by Kerner in 1996–1998 and further developed and implemented in on-line applications together with Rehborn, Aleksić, Haug, and Palmer [62–71]. A main feature of the FOTO and ASDA models is that they perform in *on-line applications without any validation of model parameters* in different environmental and traffic conditions. The FOTO (**F**orecasting **O**f **T**raffic **O**bjects) model identifies traffic phases and tracks synchronized flow. The ASDA model (**A**utomatische **S**tau**d**ynamik**a**nalyse: Automatic Tracking of Moving Jams) is devoted to the tracking of moving jam propagation.

In the FOTO model, firstly based on local measurements of traffic the local identification of the traffic phases at detector locations is performed. In on-line installations [64–71], the following simple rules are often used: (i) FOTO detects synchronized flow, when $v \le v_{\text{syn}}$; (ii) FOTO detects a wide moving jam, when $v < v_{\text{jam}}$ and $q < q_{\text{jam}}$; (iii) FOTO detects free flow, when $v > v_{\text{syn}}$, where speeds v_{syn}, v_{jam}, and the flow rate q_{jam} are model parameters. Secondly, fronts of wide moving jams ($x_{\text{up}}^{(\text{jam})}, x_{\text{down}}^{(\text{jam})}$) and of synchronized flow ($x_{\text{up}}^{(\text{syn})}, x_{\text{down}}^{(\text{syn})}$) are determined.

Finally, based on the FOTO and ASDA models the tracking and forecasting of these fronts in time and space is calculated, i.e., the positions of all fronts $x_{\text{up}}^{(\text{jam})}$, $x_{\text{down}}^{(\text{jam})}$, $x_{\text{up}}^{(\text{syn})}$, and $x_{\text{down}}^{(\text{syn})}$ as functions of time are found. Note that for traffic forecasting, historical time series at least for flow rates are necessary. This tracking is related to the *on-line* description of the upstream and downstream fronts of synchronized flow and wide moving jams as well as the average speed within these traffic phases. This tracking is also carried out *between* road detectors (or other road locations at which the phases have been identified), i.e., when synchronized flow and wide moving jams cannot be measured at all. Note that the FOTO and ASDA models enable us to predict a merging and/or a dissolution of two or more initially different synchronized flow regions and of two or more initially different wide moving jams that occur between detector locations.

If synchronized flow has been identified by the FOTO model, the upstream front location of this object is tracked by the FOTO model via a cumulative flow rate approach. We assume that due to the upstream propagation of synchronized flow whose downstream front is fixed at a bottleneck, the synchronized flow has been identified at road detector B at time $t = t_{\text{syn, B}}$. At $t > t_{\text{syn, B}}$ a time-dependence of the location $x_{\text{up}}^{(\text{syn})}(t)$ of the upstream front of synchronized flow and free flow between any two detectors A and B (flow rates measured at these detectors are denoted by q_{A} and q_{B}, respectively) can be calculated through the formula:

$$x_{\text{up}}^{(\text{syn})}(t) = \mu \Delta M(t), \tag{C.1}$$

where $\Delta M(t) = \Delta M_{\text{total}}(t)/n$, n is the number of road lanes, μ is a model parameter, $\Delta M_{\text{total}}(t)$ is the net vehicle number leaving the road section between detectors A and B that is equal to

$$\Delta M_{\text{total}}(t) = \int_{t_{\text{syn, B}}}^{t} q_{\text{B}}(t)dt - \int_{t_{\text{syn, B}}}^{t} q_{\text{A}}^{*}(t)dt \quad \text{at} \quad t > t_{\text{syn, B}}, \tag{C.2}$$

$$q_{\text{A}}^{*}(t) = q_{\text{A}}(t) + q_{\text{on}} - q_{\text{off}}. \tag{C.3}$$

If a wide moving jam has been identified, the front locations of this jam are tracked with the ASDA model. For example, the locations of the upstream and downstream fronts of the wide moving jam $x_{\text{up}}^{(\text{jam})}(t)$ and $x_{\text{down}}^{(\text{jam})}(t)$, respectively, are found through the use of Stokes's shock wave formula, i.e., *no* fundamental diagram (no flow–density relationship) is used in these formulae:

$$x_{\text{up}}^{(\text{jam})}(t) = -\int_{t_0}^{t} \frac{q_1(t) - q_{\min}(t)}{\rho_{\max}(t) - (q_1(t)/v_1(t))} dt, \quad t \ge t_0, \tag{C.4}$$

$$x_{\text{down}}^{(\text{jam})}(t) = -\int_{t_1}^{t} \frac{q_2(t) - q_{\min}(t)}{\rho_{\max}(t) - (q_2(t)/v_2(t))} dt, \quad t \ge t_1. \tag{C.5}$$

In (C.4) and (C.5), $q_1(t)$ and $v_1(t)$, $q_2(t)$ and $v_2(t)$ are the measured flow rate and average speed upstream and downstream of the jam, respectively; t_0 is the time instant when the moving jam is detected at the downstream detector, the time t_1 determines the appearance of the downstream jam front at this detector; $q_{\min}(t)$ is the measured flow rate within the jam that is usually taken as zero; $\rho_{\max}(t)$ is the vehicle density within the jam.

C.2. Simple methods for approximate reconstruction of spatiotemporal traffic dynamics

In Fig. 2(b), we have used another method (and a more simple one than the ASDA and FOTO methods) for an approximate spatiotemporal reconstruction of congested traffic between detectors. As in the ASDA and FOTO methods, the approximate reconstruction of traffic variables at road locations where none of the traffic variables can be measured is made separately between each of the pair of detectors. To understand this method, we consider a pair of detectors whose co-ordinates are $x = x_{\rm up}$ (upstream detector) and $x_{\rm down}$ (downstream) and denote traffic variables measured by these detectors by $\varphi(x_{\rm up},\ t)$ and $\varphi(x_{\rm down},\ t)$ for the upstream and downstream detectors, respectively (in a general case, $\varphi = [q,\ v,\ o]$, where q, v, and o are the flow rate, macroscopic speed, and occupancy; usually, the detectors measure only two of these macroscopic traffic variables). On the road section between these two detectors, i.e., in the co-ordinate range

$$x_{\rm up} < x < x_{\rm down} \tag{C.6}$$

we consider K *virtual* road locations ($K \gg 1$) with co-ordinates x_i that are at a small distance Δd each from another within the range (C.6), where $i = 1, 2, \ldots, K$, $\Delta d \ll (x_{\rm down} - x_{\rm up})$ and, therefore, $K = (x_{\rm down} - x_{\rm up})/\Delta d \gg 1$. Then traffic variables at each of the locations x_i are found from formula:

$$\varphi(x_i, t) = \frac{x_{\rm down} - x_i}{x_{\rm down} - x_{\rm up}} \varphi\left(x_{\rm up},\ t + \frac{x_{\rm up} - x_i}{v_{\rm c}}\right) + \frac{x_i - x_{\rm up}}{x_{\rm down} - x_{\rm up}} \varphi\left(x_{\rm down},\ t + \frac{x_{\rm down} - x_i}{v_{\rm c}}\right), \tag{C.7}$$

where $v_{\rm c}$ is a negative velocity ($v_{\rm c} < 0$) that is a constant model parameter. After the traffic variables have been calculated through formula (C.7) between all detectors, the three traffic phases F, S, and J are determined at the detector locations and virtual locations between detectors. In the case, when the detectors measure the flow rate and macroscopic speed, i.e., $\varphi = [q,\ v]$ the phases F, S, and J are approximately found as follows (Fig. 2(b)): Free flow is assumed at speed $v > v_{\rm syn}$, synchronized flow is assumed at $v \le v_{\rm syn}$, wide moving jam is assumed at $v < v_{\rm jam}$ *and* $q < q_{\rm jam}$. Note that in Fig. 2(b), $\Delta d = 100$ m, $v_{\rm syn} = 75$ km/h, $v_{\rm jam} = 25$ km/h, $q_{\rm jam} = 700$ (vehicles/h)/lane and $v_{\rm c} = -16$ km/h have been used.

It must be noted that this simple method can lead to considerable errors in the approximation of regions of synchronized flow within the pattern; therefore, the method can usually be used only for a overview of a spatiotemporal structure of a congested pattern. Rather this method, for a scientific sound analysis of spatiotemporal features of the pattern real data measured at detector locations should be used as done in Refs. [5,60].

Probably, the most simple (but often not precise enough) spatiotemporal reconstruction of traffic congested measured by road detectors can be made with a space–time approximation of the data measured at detector locations with MATLAB as this has been made in Fig. 2(a) (in this figure, the macroscopic speed as a function of detector locations and time has been interpolated between the detector locations with MATLAB-function *SURFACE* with parameter *shading interp*).

References

[1] A.D. May, Traffic Flow Fundamentals, Prentice-Hall, Inc, New Jersey, 1990.
[2] http://ngsim.camsys.com/.
[3] B.S. Kerner, in: R. Rysgaard (Ed.), Proceedings of the 3rd Symposium on Highway Capacity and Level of Service, vol. 2, Road Directorate, Ministry of Transport, Denmark, 1998, pp. 621–642; M. Schreckenberg, D.E. Wolf. (Eds.), Traffic and Granular Flow '97, Springer, Singapore, 1998, pp. 239–267; A. Ceder. (Ed.), Transportation and Traffic Theory, Elsevier Science, Amsterdam, 1999, pp. 147–171.
[4] B.S. Kerner, Phys. Rev. Lett. 81 (1998) 3797; Trans. Res. Rec. 1678 (1999) 160–167; Phys. World 12 (8) (1999) 25–30.
[5] B.S. Kerner, The Physics of Traffic, Springer, Berlin, New York, 2004.
[6] B.S. Kerner, Introduction to Modern Traffic Flow Theory and Control, Springer, Berlin, New York, 2009.
[7] W. Leutzbach, Introduction to the Theory of Traffic Flow, Springer, Berlin, 1988;
N.H. Gartner, C.J. Messer, A. Rathi (Eds.), Traffic Flow Theory, Transportation Research Board, Washington, D.C, 2001;
D.C. Gazis, Traffic Theory, Springer, Berlin, 2002;
D. Chowdhury, L. Santen, A. Schadschneider, Phys. Rep. 329 (2000) 199;
D. Helbing, Rev. Modern Phys. 73 (2001) 1067–1141;
T. Nagatani, Rep. Progr. Phys. 65 (2002) 1331–1386;
K. Nagel, P. Wagner, R. Woesler, Oper. Res. 51 (2003) 681–716;
R. Mahnke, J. Kaupužs, I. Lubashevsky, Phys. Rep. 408 (2005) 1–130.
[8] B.S. Kerner, S.L. Klenov, J. Phys. A: Math. Gen. 35 (2002) L31–L43.
[9] B.S. Kerner, S.L. Klenov, D.E. Wolf, J. Phys. A: Math. Gen. 35 (2002) 9971–10013.
[10] L.C. Davis, Phys. Rev. E 69 (2004) 016108.
[11] H.K. Lee, R. Barlović, M. Schreckenberg, D. Kim, Phys. Rev. Lett. 92 (2004) 238702.
[12] R. Jiang, Q.-S. Wu, J. Phys. A: Math. Gen. 37 (2004) 8197–8213.
[13] B.S. Kerner, S.L. Klenov, J. Phys. A: Math. Gen. 37 (2004) 1–36.
[14] B.S. Kerner, S.L. Klenov, J. Phys. A: Math. Gen. 39 (2006) 1775–1809.
[15] K. Gao, R. Jiang, S.-X. Hu, B.-H. Wang, Q.-S. Wu, Phys. Rev. E 76 (2007) 026105.
[16] L.C. Davis, Phys. A 368 (2006) 541–550.
[17] L.C. Davis, Phys. A 361 (2006) 606–618.
[18] L.C. Davis, Phys. A 387 (2008) 6395–6410.
[19] L.C. Davis, Phys. A 388 (2009) 4459–4474.
[20] L.C. Davis, Phys. A 389 (2010) 3588–3599.
[21] L.C. Davis, Phys. A 391 (2012) 1679.
[22] R. Jiang, M.-B. Hua, R. Wang, Q.-S. Wu, Phys. Lett. A 365 (2007) 6–9.
[23] R. Jiang, Q.-S. Wu, Phys. Rev. E 72 (2005) 067103.
[24] R. Jiang, Q.-S. Wu, Phys. A 377 (2007) 633–640.
[25] R. Wang, R. Jiang, Q.-S. Wu, M. Liu, Phys. A 378 (2007) 475–484.

[26] A. Pottmeier, C. Thiemann, A. Schadschneider, M. Schreckenberg, in: A. Schadschneider, T. Pöschel, R. Kühne, M. Schreckenberg, D.E. Wolf (Eds.), Traffic and Granular Flow'05, Springer, Berlin, 2007, pp. 503–508.
[27] X.G. Li, Z.Y. Gao, K.P. Li, X.M. Zhao, Phys. Rev. E 76 (2007) 016110.
[28] B.S. Kerner, S.L. Klenov, A. Brakemeier, 2007 arXiv: 0712.2711.
[29] B.S. Kerner, S.L. Klenov, A. Brakemeier, Proc. of 2008 IEEE Intelligent Vehicles Symposium, 2008, pp. 180–185; Proc. of 4th Int. Workshop V2VCOM 2008, 2008, pp. 57–63; B.S. Kerner, S.L. Klenov, A. Brakemeier 2009 E-print, arXiv:0910.0381v2; Traf. Eng. & Cont. (6) (2010) 217–222; Proceedings of the Transportation Research Board 2010 Annual Meeting (TRB, Washington DC), 2010; Paper No.: 10-0456; B.S. Kerner 2010 e-print: arXiv:1012.5159; R.-P. Schäfer, S. Lorkowski, N. Witte, J. Palmer, H. Rehborn, B.S. Kerner Traf. Eng. and Cont. 52 (5) (2011) 225–230; B.S. Kerner, H. Rehborn, J. Palmer, S.L. Klenov Traf. Eng. and Cont. 52 (3) (2011) 141–148.
[30] J.J. Wu, H.J. Sun, Z.Y. Gao, Phys. Rev. E 78 (2008) 036103.
[31] K. Gao, R. Jiang, B.-H. Wang, Q.-S. Wu, Phys. A 388 (2009) 3233–3243.
[32] B. Jia, X.-G. Li, T. Chen, R. Jiang, Z.-Y. Gao, Transportmetrica 7 (2011) 127.
[33] J.-F. Tian, B. Jia, X.-G. Li, R. Jiang, X.-M. Zhao, Z.-Y. Gao, Phys. A 388 (2009) 4827–4837.
[34] S. He, W. Guan, L. Song, Phys. A 389 (2009) 825–836.
[35] C.-J. Jin, W. Wang, R. Jiang, K. Gao, J. Stat. Mech. (2010) P03018.
[36] S. Kokubo, J. Tanimoto, A. Hagishima, Phys. A 390 (2011) 561–568.
[37] H.-K. Lee, B.-J. Kim, Phys. A 390 (2011) 4555–4561.
[38] C.-J. Jin, W. Wang, Phys. A 390 (2011) 4184–4191.
[39] J.P.L. Neto, M.L. Lyra, C.R. da Silva, Phys. A 390 (2011) 3558–3565.
[40] P. Zhang, C.-X. Wu, S.C. Wong, Phys. A 391 (2012) 456.
[41] B.S. Kerner, J. Phys. A: Math. Theor. 44 (2011) 092001.
[42] B.S. Kerner, S.L. Klenov, M. Schreckenberg, Phys. Rev. E 84 (2011) 046110.
[43] B.S. Kerner, Phys. A 355 (2005) 565–601; IEEE Trans. on Intel. Trans. Sys. 8 (2007) 308–320; Traffic Eng. Control 66 (2007) 114; Trans. Res. Rec. (2007) 30–39; Trans. Res. Rec. 2088 (2008) 80–89.
[44] S. Lee, B. Heydecker, Y.H Kim, E.-Y. Shon, J. Adv. Trans. 4 (2011) 143–158.
[45] J.-F. Tian, Z.-Z. Yuana, M. Treiber, B. Jia, W.-Y. Zhanga, Phys. A 391 (2012) 3129.
[46] M.E.M. Kimathi, Mathematical models for 3-phase traffic flow theory, Doctor Thesis, 2012. https://kluedo.ub.uni-kl.de/frontdoor/index/index/docId/2899.
[47] B.S. Kerner, S.L. Klenov, A. Hiller, J. Phys. A: Math. Gen. 39 (2006) 2001–2020; Non. Dyn. 49 (2007) 525–553; Phys. Rev. E 73 (2006) 046107.
[48] Kerner, Klenov, Phys. Rev. E 68 (2003) 036130.
[49] B.S. Kerner, S.L. Klenov, Phys. Rev. E 80 (2009) 056101.
[50] B.S. Kerner, S.L. Klenov, J. Phys. A: Theor. Math. 43 (2010) 425101.
[51] B.S. Kerner, Phys. Rev. E 85 (2012) 036110.
[52] R. Herman, E.W. Montroll, R.B. Potts, R.W. Rothery, Oper. Res. 7 (1959) 86–106.
[53] D.C. Gazis, R. Herman, R.W. Rothery, Oper. Res. 9 (1961) 545–567.
[54] G.F. Newell, Oper. Res. 9 (1961) 209–229.
[55] K. Nagel, M. Schreckenberg, J. Phys. (France) I 2 (1992) 2221–2229.
[56] R. Barlović, L. Santen, A. Schadschneider, M. Schreckenberg, Eur. Phys. J. B 5 (1998) 793–800.
[57] M. Bando, K. Hasebe, A. Nakayama, A. Shibata, Y. Sugiyama, Phys. Rev. E 51 (1995) 1035–1042.
[58] S. Krauß, P. Wagner, C. Gawron, Phys. Rev. E 55 (1997) 5597–5602;
S. Krauß, Ph.D. Thesis, DRL-Forschungsbericht 98-08, 1998. http://www.zaik.de/paper.
[59] P.G. Gipps, Trans. Res. B 15 (1981) 105–111.
[60] B.S. Kerner, Phys. Rev. E 65 (2002) 046138.
[61] J. Palmer, H. Rehborn, B.S. Kerner, Traf. Eng. and Cont. 52 (4) (2011) 183–191.
[62] B.S. Kerner, H. Rehborn, M. Aleksić, A. Haug, Transp. Res. C 12 (2004) 369–400.
[63] B.S. Kerner, H. Rehborn, H. Kirschfink, German Patent DE 196 47 127 C2, 1998. US Patent US 5861820.
[64] B.S. Kerner, German Patent DE 199 40 957 C2, 1999.
[65] B.S. Kerner, German Patent DE 199 44 075 C2, 1999. USA Patent US 2002045985; Japan Patent JP 2002117481.
[66] B.S. Kerner, M. Aleksić, U. Denneler, German Patent DE 199 44 077 C1, 1999.
[67] H. Rehborn, J. Palmer, Straßenverkehrstechnik (8) (2008) 463–470.
[68] H. Rehborn, J. Palmer, Traf. Eng. & Cont. 49 (2008) 261–266.
[69] H. Rehborn, J. Palmer, Proceedings of IEEE Intelligent Vehicles Symposium, Eindhoven, 2008.
[70] J. Palmer, H. Rehborn, L. Mbekeani, Proceedings of 15th World Congress on Intelligent Transport Systems, New York, 2008.
[71] H. Rehborn, S.L. Klenov, in: R.A. Meyers (Ed.), Springer Encyclopedia of Complexity and System Science, Springer, Berlin, 2009.